REVIEW ARTICLE OPEN

Check for updates

Recent advances in flexible noninvasive electrodes for surface electromyography acquisition

Lian Cheng[1,2], Jun Li[1,2]✉, Aiying Guo[1] and Jianhua Zhang[1,2]✉

Surface electromyography (sEMG) is used to detect and analyze human muscle biopotential. Recently, flexible noninvasive electrodes (FNEs) have emerged to extract bioelectrical signals from individual bodies. For FNEs to be deployed as a central component of physiological signal acquisition, the quest for elevated signal-to-noise ratio and density is compelling owing to the small amplitude of sEMG. Herein, we review recent progress in FNEs for sEMG acquisition. We summarize the needed properties of FNEs, compare the differences between passive electrodes and active electrodes and exemplify applications of FNEs. We also conclude the current challenges and future opportunities in sEMG acquisition.

npj Flexible Electronics (2023)7:39 ; https://doi.org/10.1038/s41528-023-00273-0

INTRODUCTION

Flexible electronics[1], such as wearables, epidermal devices, and implantable electronics, have become attractive in the fields of human health monitoring[2–4], stimulation systems[5], and human–machine interfaces[6–8]. Flexible electrodes serve as the fundamental component of flexible electronics and are designed to monitor electroencephalogram (EEG)[9–11], electromyography (EMG)[12], and electrocardiogram (ECG) measurements[13,14]. EEG provides valuable insights into the human brain's condition, which is used in various health domains, such as fatigue detection, sleep monitoring, and mental health diagnosis. EEG electrodes are placed on the scalp to detect weak electrical signals generated by the discharge of neurons in the cerebral cortex (5–300 μV, 0.5–100 Hz)[15]. Cardiovascular disease poses a significant risk to global human health, but it can be prevented and diagnosed through a straightforward and effective method: ECG monitoring. ECG electrodes are applied to the chest to monitor heart activity by measuring the electrical signals of heart contraction and relaxation (10 μV–4 mV, 0.05–100 Hz)[16]. EMG signals, however, have a broader bandwidth of 0 to 500 Hz and values of 0–1.5 mV. Given the weakness of EEG, ECG, and EMG signals, these electrodes require high sensitivity, precision, and resolution to accurately capture small changes in physiological electrical activity. EMG is widely used to obtain information on the clinical status of muscles and as a source of prosthetic control information. Flexible electrodes for EMG measurements can be broken into two categories: (1) flexible electrodes that work in vivo (iEMG)[17], and (2) flexible electrodes that are used for measurements outside the organism (sEMG)[18–21]. iEMG measurement requires the implantation of needle electrodes inside the muscle, on the contrary, sEMG measurement only requires electrodes touching the skin on the muscle. Clear information about the local behavior of muscle fibers can be obtained through iEMG electrodes. Whereas a broader view of the transient state of the muscle can be monitored by the sEMG electrodes. Moreover, invasive electrodes for collecting EMG signals can cause physical and mental damage to the tester in many cases, such as biofeedback, ergonomics, sports, and space medicine, etc. Therefore, flexible and noninvasive sEMG electrodes are preferred over iEMG electrodes as they provide information on overall muscle activity. Due to their noninvasive and low-cost properties, sEMG recordings have been used in monitoring neuromuscular activities (Fig. 1 and see refs. [2,19,22–31]).

Traditional bipolar sEMG electrodes can only provide a one-dimensional time signal, which fails to distinguish or characterize individual motor unit action potential waveforms. Furthermore, the various physiological electrical signal measurement instruments currently used in hospitals have become more advanced. However, with the increasing demand for bioelectric signals in health testing, the need to capture sEMG signals at the few millivolts level is crucial[32–36]. Based on these considerations, a multichannel electrode with a high signal-to-noise ratio (SNR) is desirable for collecting sEMG signals[37–39]. To meet these requirements and ensure the quality of bioelectrical signals, flexible thin-film transistors (TFT) technology can be employed to improve the transmission quality and SNR of sEMG signals.

So far, there has been extensive research conducted on EEG and ECG electrodes, whereas EMG electrodes have received very little attention in terms of detailed reviews[40–42]. This comprehensive review focuses primarily on the development of emerging flexible noninvasive electrodes (FNEs) for sEMG acquisition (Fig. 2). The review starts with an introduction to the latest advancements in FNEs, followed by a detailed discussion of different sorts of materials, structures, and properties of the electrode, including adhesiveness, breathability, flexibility, long-term durability, biocompatibility and biodegradability, and high SNR. The following section provides an in-depth analysis of the differences between passive and active FNEs. It discusses various TFT materials and amplifiers used in active FNEs, providing detailed classification and analysis. Eventually, the application of wearable sensors for healthcare and human–machine interfaces (HMI) is presented, outlining the challenges and prospects for FNEs in sEMG signals acquisition.

PROPERTIES OF sEMG ELECTRODES

It is noteworthy that the durable stability of human skin is critical for continuous monitoring of vital sign signals. Skin bioelectronic for next-generation electronics are required to

[1]School of Microelectronics, Shanghai University, 201800 Shanghai, China. [2]Key Laboratory of Advanced Display and System Applications, Ministry of Education, Shanghai University, 200072 Shanghai, People's Republic of China. ✉email: lijun_yt@shu.edu.cn; jhzhang@oa.shu.edu.cn

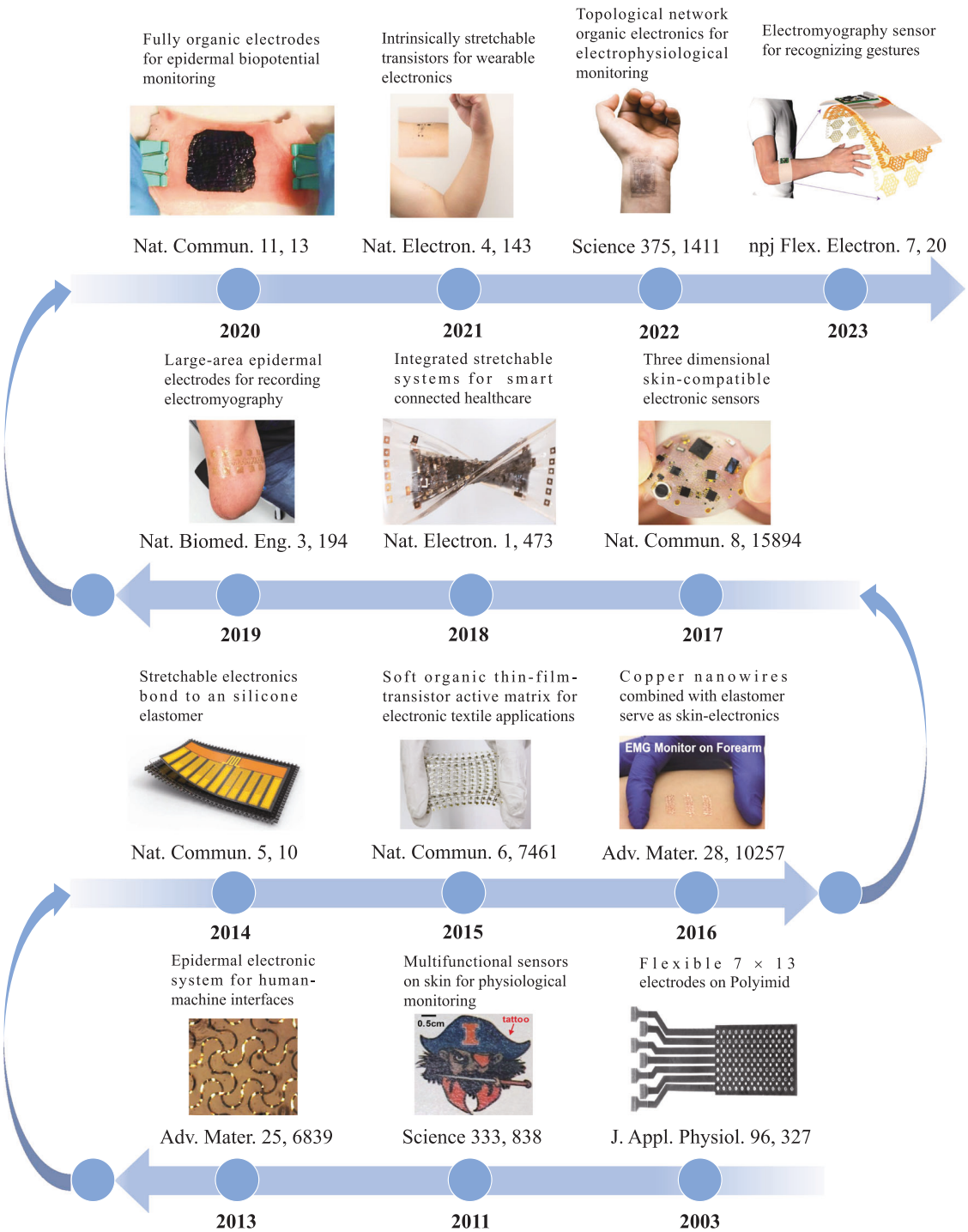

Fig. 1 Timeline of developments in flexible noninvasive electrodes. Reproduced with permission[19]. Copyright @ 2003, American Physiological Society, Reproduced with permission[22]. Copyright @ 2011, American Association for the Advancement of Science, Reproduced with permission[23]. Copyright @ 2013, Wiley-Blackwell, Reproduced with permission[24]. Copyright @ 2014, Springer Nature, Reproduced with permission[25]. Copyright @ 2015, Springer Nature, Reproduced with permission[26]. Copyright @ 2016, Wiley-Blackwell, Reproduced with permission[2]. Copyright @ 2017, Springer Nature, Reproduced with permission[27]. Copyright @ 2018, Springer Nature, Reproduced with permission[28]. Copyright @ 2019, Springer Nature, Reproduced with permission[29]. Copyright @ 2020, Springer Nature, Reproduced with permission[30]. Copyright @ 2021, Springer Nature, Reproduced with permission[31]. Copyright @ 2022, American Association for the Advancement of Science, Reproduced with permission[238]. Copyright @ 2023, Springer Nature.

possess important characteristics in superb adhesion[9,24,43–50], breathable[28,51–57], and flexibility[21,58–60] to guarantee stable properties through permanent health monitoring. Therefore, stable materials are considered a key platform for monitoring human health.

Adhesion

Sufficient adhesion to the skin is crucial for long-term recording in flexible electronic devices. The close contact between the electrode and the deformed skin can help to maintain consistent contact areas during movement, eliminate motion artifacts, and

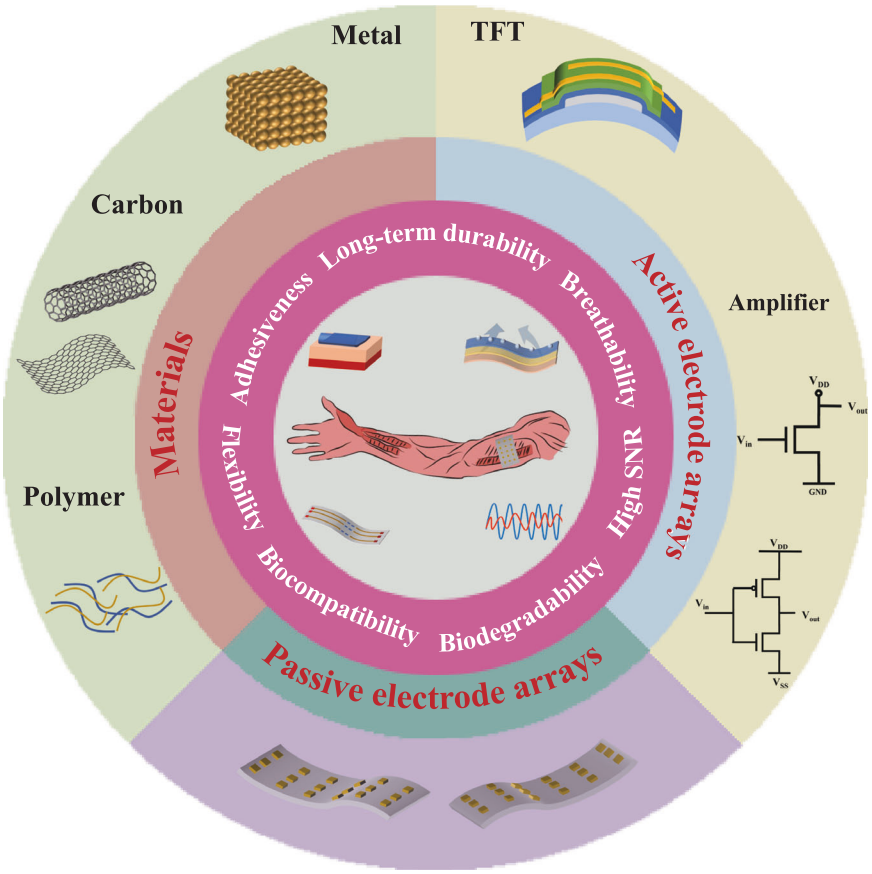

Fig. 2 Recent advances in flexible noninvasive electrodes for sEMG acquisition.

reduce the interface impedance of the skin-mountable electrode, thus enhancing high SNR and accuracy. Furthermore, sEMG electrodes are required to maintain adhesive properties under sweaty conditions, which is inevitable during long-term monitoring and sports. In order to maintain close contact between the electrode and the skin, various methods can be undertaken, such as using a bio-adhesive, manufacturing microstructures electrodes, and preparing pressure-sensitive adhesives[9].

To achieve good adhesion between human skin and FNEs, biocompatible adhesives can be prepared and placed on the human epidermis. In general, there are several types of adhesives, including water-soluble tapes[47], bandage adhesives[48], silicone adhesives[24], and adhesives developed in the laboratory[29]. For example, Yeo and his co-workers developed flexible and stretchable epidermal electronic systems (EES) that fit tightly to human skin via van der Waals forces[48], and can measure both ECG and EMG signals. The EES was integrated by direct printing on the forearm and encapsulation with spray-on-bandage (Fig. 3a). The adhesive force of the spray-on bandage was 0.98 ± 0.03 N, which is close to the adhesive forces of traditional medical dressings. Therefore, the biocompatible and adhesive EES are extremely suitable for physiological monitoring. In 2014, Jang's group proposed stretchable electronic systems with adhesion by bonding to an ultralow modulus silicone (UL-Sil) (Fig. 3b)[24]. The silicone had a low modulus of 3.0 kPa and outstanding adhesion to the skin of 1.5 kPa. Attributed to the soft surface and adhesion the UL-Sil, electronic systems can not only firmly adhere to the skin, but also be easily peeled off. This allows for multiple uses of the electronic systems without damaging their performance. To further reduce the impedance between electrodes and the skin, Yang et al.[61] utilized lower impedance conducting polymers polypyrrole (PPy) and combined them with silk fibroin (SF) to form an interlocking structure, resulting in a conformal and adhesive polymer electrode (CAPE) (Fig. 3c). Compared with Ag/AgCl electrodes detaching from the wet surface of a pig heart, the CAPE was able to sustain 100 g of weight when applied to the same surface. At 52.8% relative humidity, the adhesion energy of CAPE is 17 J m^{-2}, which is similar to that of Ag/AgCl electrodes. Therefore, CAPE can collect stable and reliable ambulatory electrophysiological signals during long-term sports management. Zhang et al.[29] prepared electrodes made of conductive poly(-ethylenedioxythiophene):poly(styrenesulfonate) (PEDOT:PSS), stretchable waterborne polyurethane (PU), and adhesive. The electrodes can attach tightly on the skin, whether it is dry or wet, smooth or hairy. It is an experiment that the adhesion force of a pristine electrode to the skin is 0.43 N cm^{-1}. Therefore, the electrodes with high adaptability can precisely measure physiological electrical signals under various conditions.

In addition to the above-mentioned methods to enhance adhesion, creating various microstructures is also an effective method for developing adhesive electrodes[43,44,49,50]. For example, Chen et al.[44] prepared nanopiles fabricated under the metal film to form the interlocking layer inspired by stretching out fractal root trees (Fig. 3d). The tensile adhesion strength was used to quantitatively reflect the adhesion. The adhesion strength of nanopile film was at least one order of magnitude higher than that of the other two control experimental groups. Thus, the nanopile interlocking can not only improve the adhesion but also achieve the enhancement of stretchability. Lamellibranchia, such as oysters and or mussels, can highly adhere to rock surfaces. Inspired by this, Ye et al.[62] modified the poly(dimethylsiloxane) (PDMS) backbone with soft and hard domains to create electrodes for recording electrophysiological signals (Fig. 3e). It is an experiment that the adhesive electrodes exhibited maximum

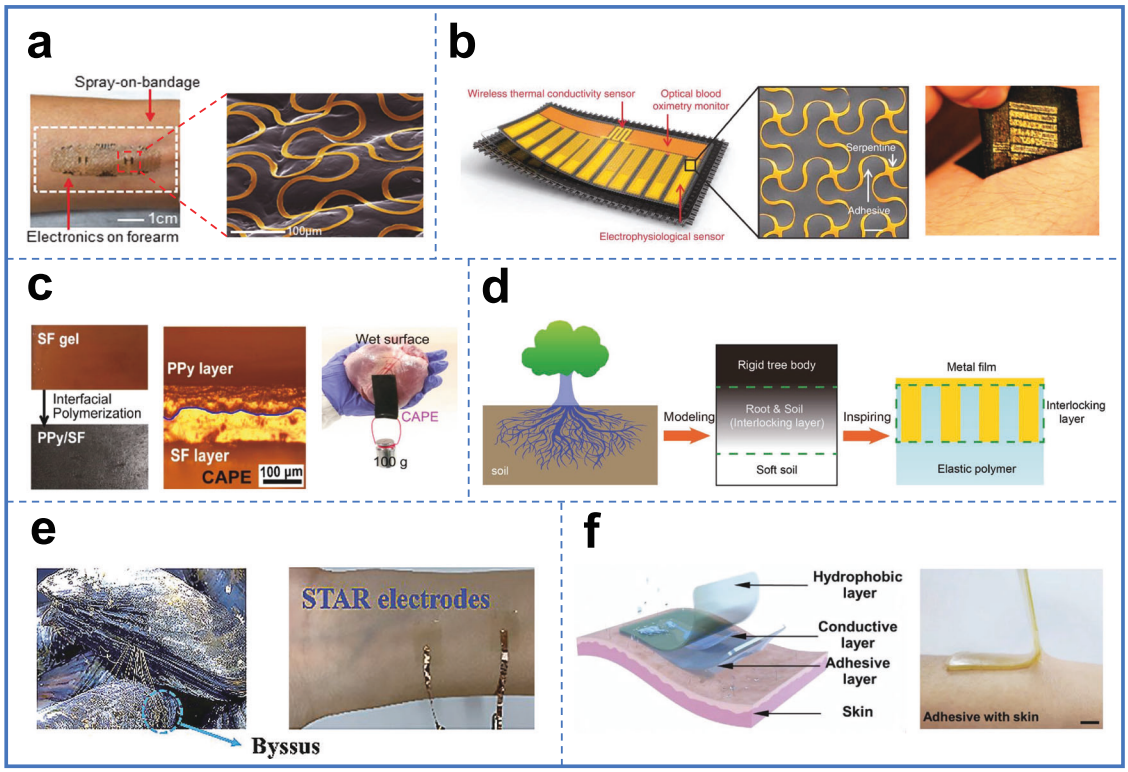

Fig. 3 Electrodes with adhesion. a The multifunctional epidermal electronic system attached to the human skin. **b** A schematic illustration of a device (left) and detachment of the device from the human skin (right). **c** The schematic diagram and physical diagram of CAPE. **d** The adhesion structure inspired by tree roots. **e** The schematic of a Lamellibranchia-inspired electrode. **f** Schematics of the biosensor and high adhesion between electrodes and the human skin. Scale bars: 5 mm. **a** Reproduced with permission[48]. Copyright @ 2013, Wiley-VCH. **b** Reproduced with permission[24]. Copyright @ 2014, Springer Nature. **c** Reproduced with permission[61]. Copyright @ 2020, American Chemical Society. **d** Reproduced with permission[44]. Copyright @ 2016, Wiley-VCH. **e** Reproduced with permission[62]. Copyright @ 2021, Royal Society of Chemistry. **f** Reproduced with permission[9]. Copyright @ 2022, Wiley-VCH.

adhesive strengths of 30 kPa on pig skin. The adhesiveness of the electrodes can be attributed to two factors: (1) the use of 4,40-methylenebis(phenyl isocyanate) as the hard domain, which can form hydrogen bonds with hydrophilic surfaces containing oxygen-containing functional groups; and (2) the use of aliphatic disulfide linkages as the soft domain, which can interact with metal or biological tissues to provide further adhesive force.

Besides, chemical modification of the substrate or electrode can increase viscosity[63–67]. Inspired by the adhesion mechanism of mussels and barnacles, Yang et al.[9] prepared a biosensor using adhesive and hydrophobic bilayer hydrogels (AHBH) as well as an electronically conductive composite electrode, namely AHBH-ECC electrode. This AHBH-ECC electrode was able to collect high-quality sEMG signals even under conditions of heavy sweating (Fig. 3f). The AHBH-ECC electrode had an outstanding adhesion force of 59.7 N cm^{-1} owing to the adhesion mechanism of catechol groups and electrostatic interactions. In addition, the AHBH-ECC electrode on wet skin is maintained at 44.1 N m^{-1}. To verify the strong adhesion of the AHBH-ECC electrode, adhesion tests were conducted on the AHBH-ECC electrode and the commercial Ag/AgCl gel electrode simultaneously. The results indicated that the AHBH-ECC electrode can firmly adhere to the skin after spraying several times, whereas the Ag/AgCl electrode was detached.

Breathability

In terms of breathability, the accumulation of sweat can increase motion artifacts and contact impedance, and irritate the skin, which can result in device failure. Similarly, skin allergies and irritation can occur with long-term monitoring due to the accumulation of water vapor and sweat[54]. Therefore, FNEs with breathability are preferred to enhance the biocompatibility of the device and prevent the adverse effects of sweat on the quality of collected sEMG signals. Thus, breathability is an essential factor that should be considered when monitoring sEMG signals[57,68–71].

The nanomesh structure can facilitate skin breathing, which is crucial for alleviating stuffiness and inflammation of the skin. Miyamoto et al.[57] prepared nanomesh electronics made of polyvinyl alcohol (PVA) (Fig. 4a). Attributed to the high permeability of the porous structure of the nanomesh electronics, no irritation or inflammation of the skin was observed during one week of testing. To verify the contribution of the nanomesh structure to breathability, films made of the nanomesh structure and other materials were placed separately at the opening of bottles filled with pure water (1 g). The breathability of these films was analyzed by measuring the loss of water. Both the bottle with and without nanomesh electronics reduced in weight at the same rate (water both evaporates within a week). Hence, nanomesh electronics demonstrated outstanding water vapor permeability. Kwon et al.[52] developed the breathable multichannel large-area epidermal electronic system (L-EES) for high-quality sEMG signal monitoring of spinal cord injury patients, which was highly conductive and biocompatible (Fig. 4b). The integration of nanomembrane electrodes with elastomer and fabric enabled the L-EES to have breathability, as well as exhibit anon-cytotoxic and lower allergic reactivity compared to traditional gel electrodes. They tested the breathability of L-EES and found that its WVTR value (3.13 ± 0.18 g m^{-2} h^{-1}) was comparable to that of commercial Tegaderm, suggesting that it could be used for long-term EMG recording without causing skin breakdown. Currently, the sizes of FNEs are typically limited to a few square centimeters[72–75]. To

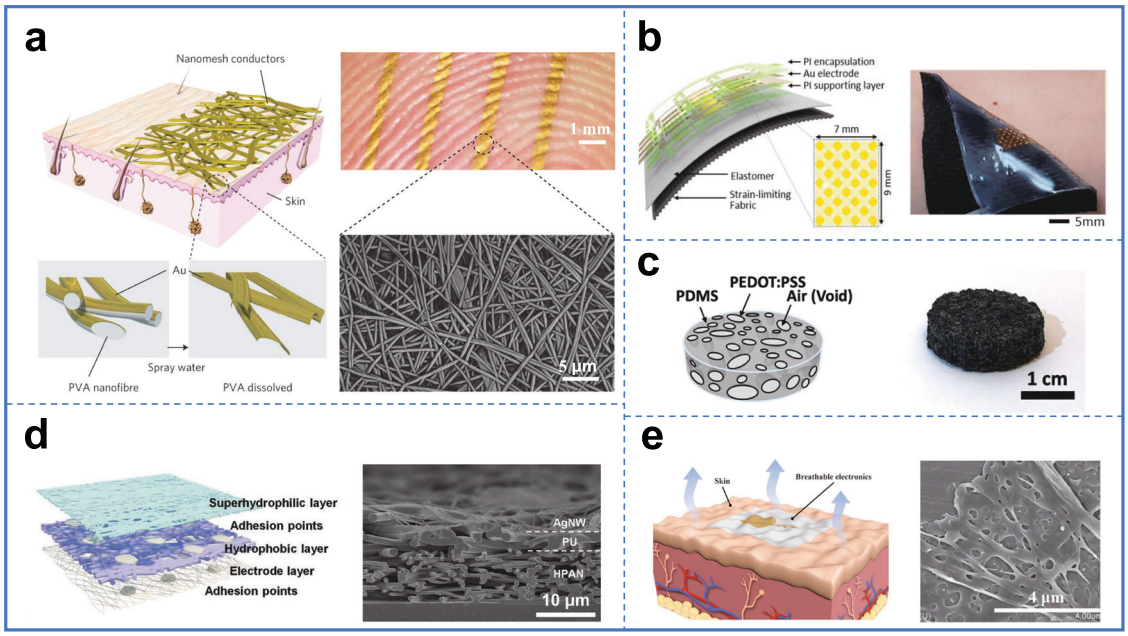

Fig. 4 Electrodes with breathability. The schematic illustration and the photograph of **a** the nanomesh electronics, **b** the large-area epidermal electronic system, **c** the sponge electrode, **d** Janus textile electrode, **e** e-tattoo. **a** Reproduced with permission[57]. Copyright @ 2017, Springer Nature. **b** Reproduced with permission[52]. Copyright @ 2020, Elsevier. **c** Reproduced with permission[55]. Copyright @ 2022, American Chemical Society. **d** Reproduced with permission[76]. Copyright @ 2022, Wiley-VCH. **e** Reproduced with permission[77]. Copyright @ 2023, Elsevier BV.

overcome the problem, Tian et al. prepared large-area breathable FNEs with a microperforated soft silicone layer enabling reliable and robust recording of sEMG signals[28]. The support structure of these breathable FNEs consisted of a tack-free membrane that can be easily detached and a heavy-duty silicone adhesive. The bilayer soft-support design allows for adjustment of the water vapor transmission rate, providing device protection according to user requirements. The results indicated that the water vapor transmission rate of the breathable FNEs (>10 g m^{-2} d^{-1}), surpassing that of PDMS films. This significant finding highlighted the superior breathability of FNEs and their potential for extensive coverage over superficial muscle groups to monitor sEMG signals. Furthermore, the remarkable feature of breathability makes these FNEs suitable for application on sensitive and scarred tissue, expanding their versatility and applicability.

Creating a porous structure to achieve breathability and promote sweat evaporation is a common strategy used in wearable devices. Lo et al.[55] reported the sponge electrode with high impedance and SNR for the acquisition of high-quality bioelectrical signals (Fig. 4c). The sponge electrode owned a lower contact impedance than that of traditional Ag/AgCl electrodes because the sponge electrode with abundant micropores enhanced the contact area and the breathability of the skin electrode. Through the analysis of sEMG data, the porous electrodes had high SNR of 60 dB, which was higher than that of the Ag/AgCl electrode. As a result, the sponge electrode remained in outstanding contact with skin electrode due to the substantial gel stored inside the electrode, which reduced contact impedance and promoted the SNR of sEMG signals. In 2022, Yang et al.[76] proposed porous textile electrodes designed with directional perspiration penetration for capturing bioelectrical signals. The multilayer electrodes were composed of super-hydrophilic-hydrolyzed-polyacrylonitrile (HPAN), PU, and silver nanowires (AgNWs). The porous structure of textile electrodes was created by electrospinning the HPAN layer and the PU layer (Fig. 4d). Moreover, the conductive network was formed by fibers with dispersed AgNWs through vacuum filtration. Due to their hydrophilic gradient structure, the textile electrodes exhibited high water vapor permeability and were able to evaporate sweat within seconds. The corresponding water vapor transmission rate (WVTR) can be calculated from the measured weight loss (Δm) using the formula: WVTR $= \Delta m/(A \times T)$, where A is the material area and T is the testing time. The textile electrode was found to possess a WVTR of 1748.09 g m^{-2} d^{-1}. It is noteworthy that the electrode had a strong adhesion force with human skin (43.08 N m^{-1}) and outstanding flexibility (strain >500%). Monitoring sEMG signals precisely and continuously played an important part in rehabilitation therapy. Zheng et al.[77] prepared a breathable electronic tattoo (e-tattoo) consisting of porous thermoplastic polyurethane (TPU) substrate and conductive AgNWs layer (Fig. 4e). The e-tattoo, characterized by an abundance of voids, exhibits breathability, allowing for comfortable and long-term attachment to the skin. The e-tattoo demonstrates a remarkable breathability of 20.5 mg cm^{-2} h^{-1}, surpassing the breathability of medical tape (2.3 mg cm^{-2} h^{-1}) by a significant margin. By adhering the e-tattoo to a specific area of the human body, it becomes capable of detecting EMG signals.

Flexibility

The growing global interest in FNEs can be attributed to their ability to closely match human tissues, minimizing discomfort and irritation during measurement[78,79]. In addition, the flexibility of these electrodes not only helps to prevent damage to the skin and underlying tissues but also enhances wearable comfort. Skin is a soft organ, which typically has Young's modulus ranging from 0.5 to 1.95 MPa[80]. To ensure biocompatibility and prevent damage, on-skin electrodes must match the low Young's modulus of human skin. By using flexible electrodes with similar mechanical properties, they can conform to the skin's curves, ensuring accurate signal transmission and a comfortable wearing experience.

There are generally two ways to obtain flexible electrode materials. One way is for the electrode material itself to possess flexibility. For example, liquid metals[81] and conductive polymers[82]. These materials can harness their intrinsic mechanical properties

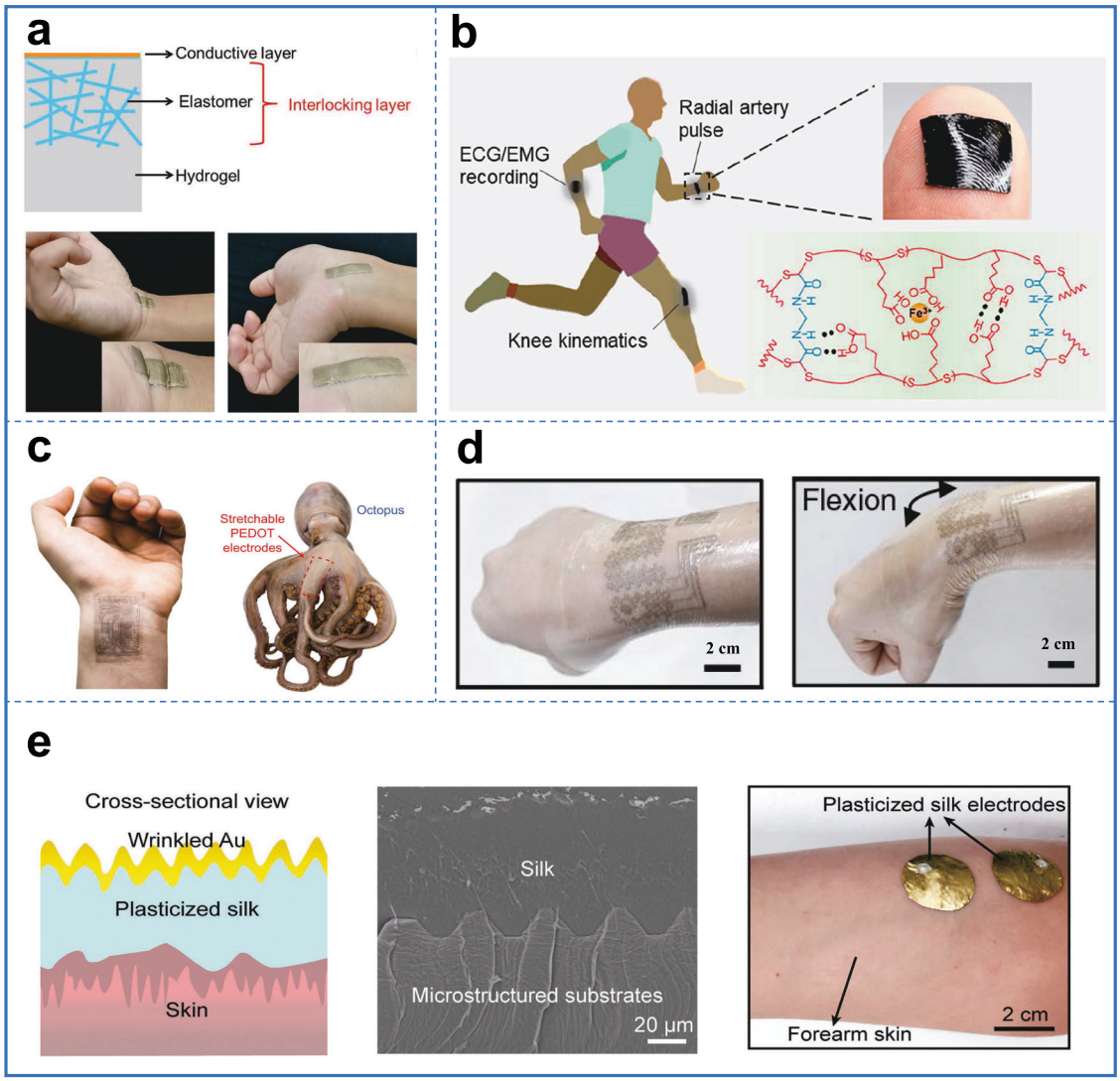

Fig. 5 Electrodes with flexibility. a The schematic and pictures of mechanically interlocked electrodes. **b** The schematic illustration of patch electrodes for physiological signals recording. **c** Photographic images of the conformal interface between flexible electrodes and tissues. **d** The flexible device following the contour of the joints of the wrist. **e** A scheme and photos of on-skin electrodes based on plasticized silk protein. **a** Reproduced with permission[83]. Copyright @ 2020, Wiley-VCH Verlag. **b** Reproduced with permission[84]. Copyright @ 2022, American Chemical Society. **c** Reproduced with permission[31]. Copyright @ 2022, American Association for the Advancement of Science. **d** Reproduced with permission[59]. Copyright @ 2018, Springer Nature. **e** Reproduced with permission[89]. Copyright @ 2018, Wiley-Blackwell.

to achieve flexibility without additional modifications. Hydrogels, as common conductive polymers, with high water content and remarkable softness (1–100 kPa), have gained significant attention in bioelectronics. Pan et al.[83] synthesized highly flexible interlocked hybrids by assembling conductive elastomeric webs with hydrogels. The hybrid electrode, with Young's modulus of 11.5 kPa, is suitable for an on-skin application, offering high adhesiveness and mechanical softness. This enables easy and reliable adherence to the skin, facilitating the accurate recording of EMG and ECG signals. During wrist movements, the hybrid electrode remained firmly adhered to the skin without any detachment. Meanwhile, wrinkles appeared on its surface, confirming its mechanical softness (Fig. 5a). Cheng et al.[84] innovatively created patch electrodes by integrating a percolation network of carbon nanotubes (CNTs) percolation network into a synthesized supramolecular polymer (Fig. 5b). The epidermal patch seamlessly integrates with the skin's texture, creating an interlocking effect at the interface, thanks to its skin-like softness (Young's modulus ~0.1 MPa) and its ability to adapt to localized curvature. The attributes enable the patch electrodes to detect high-quality biopotential and biomechanical signals. Jiang et al.[31] created biocompatible and soft electrodes through the incorporation of topological networks into conductive polymer materials. As polyrotaxane content increased, lower Young's modulus was obtained (from 2.5–3 GPa to 0.5–1 MPa), indicating that polyrotaxane can reduce the overall film stiffness. The FNEs array, seamlessly conformed to the contours of human skin, enabling the accurate recording and detection of sEMG signals (Fig. 5c). Furthermore, the FNEs array can records octopus muscles with larger deformations than human muscles, advancing the use of sEMG signals in soft-bodied robotics.

Structural designs, such as serpentine[85], kirigami[86], fabric[87], and waves[88] offer an alternative approach to achieving flexibility. These designs introduce specific structures that can impart a certain level of flexibility to rigid devices. Utilizing elastomeric media, conductive nanomaterials can form a percolation network in nanocomposites, providing a flexible substitute for rigid and fragile traditional metallic materials. Choi et al.[59] prepared serpentine-shaped Ag–Au nanocomposites with the flexibility to capture sEMG signals. The drying process led to phase separation,

resulting in the formation of microstructures within the nanocomposite, thereby enhancing the flexibility of electrodes. An increased weight fraction of hexylamine is inclined to induce phase separation, thus enhancing the softness of the electrode. Specifically, when the weight fraction of hexylamine is raised to 0.4, maintaining a constant weight ratio of 60:40 for Ag–Au nanowires:poly(styrene-butadiene-styrene), there is a substantial decrease in Young's modulus (<40 MPa), accompanied by a notable improvement in softness. The Ag–Au electrode exhibits remarkable flexibility, enabling it to conform seamlessly to the curves and contours of flexible joints like the wrist (Fig. 5d). The Ag–Au nanocomposite electrodes were conformally adhered to the human skin, effectively minimizing the gap between the electrode and the skin surface for the acquisition of high-quality bioelectrical signals during the monitoring process. Chen et al.[89] enhanced the flexibility of metal-film electrodes by incorporating wrinkled structures onto a soft silk protein substrate (Fig. 5e). By introducing 30 wt% $CaCl_2$ and exposing the material to ambient moisture, the initially rigid silk protein underwent plasticization, resulting in a significant reduction in Young's modulus from 5–12 GPa to 0.1–2 MPa. This is because the combination of thin-film metallization and the formation of wrinkled structures after hydration resulted in the generation of highly flexible electrodes. The silk electrodes demonstrated comparable EMG signal amplitudes to the commercial gel electrodes, confirming their effectiveness, albeit with a slightly lower SNR of 17.17 dB compared to the 17.95 dB of the commercial gel electrodes.

Biocompatibility and biodegradability

For FNEs in direct contact with human skin, prioritizing user comfort, health safety, and unrestricted daily activities is essential[90]. Biocompatibility and biodegradability are essential factors to be considered, especially for long-term applications. Thus, FNEs should possess a chemically adaptable composition that can accommodate various biochemical environments, including sweat and interstitial fluid.

Natural biopolymers with biocompatibility and biodegradability have garnered significant research attention for their integration with conductive components in biocompatible conductors. Cellulose, alginate, silk, and gelatin are commonly utilized natural biopolymers conductors in the field of soft bioelectronics. Cellulose is the most abundant natural polymeric material. Inspired by the leaf homeostasis system, Kim et al.[91] pioneered the development of a cellulose biosensor. This biosensor not only offers protective capabilities, sensory functions, and self-regulation but also ensures a high level of biosafety. Wet adhesion of the cellulose membrane (CM) on hairy skin is 7.18 ± 1.79 kPa. Notably, the CM exhibits considerably improved electrical properties, while swollen for 8 h. As a result, after expansion in a saline solution, the mesoporous CM can transform into a self-stabilizing material with high ion conductivity, flexibility and stability, appropriate adhesion, and self-healing properties. Even after undergoing 10,000 bending cycles at a radius of 3.0 mm, the conductivity of the CM remained unchanged, demonstrating its exceptional electrical stability. During the 1-h monitoring period, the CM consistently provides high-quality EEG data as demonstrated in the average results of an 8-h continuous recording conducted daily over a span of 7 days. Silk, as a commercialized natural protein fiber, is renowned for its mechanical properties, good biocompatibility, and biodegradability. It has been extensively utilized in flexible electrodes[89]. The robust adhesive design commonly found in skin-mounted devices can pose challenges during removal, resulting in skin irritation, discomfort, and potential harm to the wound area. In response to this issue, Zhang et al.[92] showed biocompatible and flexible transient epidermal electronic, which consisted of self-adhesive conductors with genetically engineered plasticized silk and genetically engineered plasticized copolymer (GEPC) as substrates. The plasticized double-network protein-based copolymer exhibited characteristics such as biocompatibility, flexibility, strong adhesion to the skin, and water-triggered transiency. This copolymer was composed of silk fibroin as the framework, genetically engineered resilin protein as the modifier, and glycerol as the plasticizer. It is worth noting that the remarkable adhesion between the GEPC substrate and the skin, capable of supporting a weight of 400 g, even on rough and hairy skin surfaces. After wearing the transient epidermal electronic for 6 h, the volunteers had almost no residue or irritation on their hands, demonstrating the biocompatibility of the patch. In addition, the designed copolymer film possesses water-triggered detachment properties and water degradability, which facilitates the application of biocompatible conductors in skin-based bioelectronics that require easy detachment after a specified lifespan. This study offers promising material advancements for long-term health monitoring in skin bioelectronics. Gelatin is derived from the hydrolysis of natural animal collagen, which exhibits biocompatibility, biodegradability, easy processability, and low cost. Lee et al.[11] presented self-adherent, biocompatible, and biodegradable hydrogel electrodes composed of gelatin and PEDOT:PSS for electrophysiological signal measurement. The adhesion force of hydrogel electrodes is measured to be 0.22 ± 0.03 N cm^{-1} when the hydrogel-forming solutions contain a 1 wt% concentration of dimethyl sulfoxide.

To address the issue of chemical biocompatibility, another commonly employed approach is to encapsulate the device entirely in biocompatible materials such as polyimide (PI) or PDMS. For example, Cai et al.[93] successfully developed a quadra-layered ionotronic hybrid that combines an ionic hydrogel and a strain-sensitive double metallic nanofilm on an elastomer, with PDMS encapsulation. The SNR signal of sEMG measured by the hybrids is 32.2 dB. In addition, these hybrids demonstrated significantly lower impedance with the skin across the entire frequency range, as well as a low impedance of 8 kΩ at a frequency of 1 Hz.

Long-term durability

In many wearable applications, an instantaneous degradation of the device performance could occur, resulting in the permanent failure of devices. Thus, the long-term stability of skin electronics holds significant importance for continuous health monitoring. Achieving long-term stability entails considering various aspects of characteristics, such as biocompatibility, breathability, electrical-mechanical stability, etc. Efforts are underway to develop stable materials and manufacturing methods to accommodate on-demand, continuous health monitoring, and diagnostics.

An alternative method to ensure long-term stability is by employing a silicone shell to encase the device[94]. Gandla et al.[95] prepared a patch-based large-area stretchable sensor array packaging in Ecoflex, which has a low modulus (50 kPa), reversible adhesion to the skin (3.3 kPa), and high stretchability (>100%). The sensor array possessed water-permeability, which is crucial for the long-term wear of sensors as it enables the continuous release of sweat to prevent skin allergies or infection. Over 10,000 cycles of stretching from the initial state (0%) to the final state (30%), the sensor exhibited minimal variation in relative resistance, indicating its durability. Another approach to achieving long-term stability is the development of FNEs with self-healing capabilities[96,97]. Song et al.[98] demonstrated the preparation of a conducting composite by combining a self-healing polymer with graphene. The composite exhibited reliable electrical performance, maintaining its functionality even after undergoing 200 cycles of self-healing at a strain of 50%. Importantly, the optimized composite exhibited the ability to restore not just its mechanical properties, but also its electrical properties following damage through self-healing. Kim et al.[99]

fabricated a robust and stretchable electronic textile. To assess its durability, cyclic tests were conducted, subjecting the sample to 1000 cycles at a 25% strain. Consequently, the effective stress relaxation of the kirigami pattern led to a less than 0.25-fold increase in the resistance of the electronic textile.

High SNR

In electrophysiological signal acquisition, the SNR is an important criterion for the quality of the acquisition. SNR is defined as the ratio of signal energy to noise energy and can be expressed by the formula: $\mathrm{SNR(dB)} = 10_{10}\left(\frac{P_{\mathrm{signal}}}{P_{\mathrm{noise}}}\right)$, where P_{signal} is the peak-to-peak voltage of the electrophysiology signal and P_{noise} is the peak-to-peak voltage of the noise.

Notably, the selection of the electrode size, shape, material, and interelectrode distance is critical for obtaining high SNR such as DC potential and environment noise. Passive FNEs have a high spatial and temporal resolution. However, their large number of wires causes crosstalk between signals and increases the interference from external electromagnetic waves, which leads to a significant decrease in the SNR of the sEMG signal. The active circuit based on TFTs can achieve signal pre-processing and scalable design of electrodes, which is useful for improving the SNR of sEMG signals.

MATERIALS ELECTRODES AND STRUCTURAL DESIGNS

Materials are the basis of electrodes, which plays an important part in the performance of the electrode. Materials electrodes can be mainly categorized into metal electrode material[52,100], carbon electrode material[101,102], and conductive polymers. The corresponding electrode structures are various, such as serpentine, fractal geometry designs and three-dimensional structures, and so on. In this section, we descript the acquisition of sEMG signal by using flexible electrodes made of the above three materials, respectively.

sEMG electrodes with various materials

Metal-based electrodes. Metal-based electrodes with conductivity and low skin-electrode impedance are highly suitable for acquiring sEMG signals, as they effectively enhance the amplitude of charge transfer[57,58]. By designing special structures, it is possible to achieve ultrathin electrodes with thicknesses down to the nanometer level. It is worth mentioning that metal material electrodes can be manufactured through technologies with relatively low costs, such as magnetron sputtering and electrochemical deposition[103–105].

In 2022, Zou et al. and co-workers fabricated directly printed customized microstructure-enhanced patterned electrodes, which can capture human electrophysiological signals[106]. The gold/chrome (Au/Cr) electrode layer was deposited on the polyethylene terephthalate (PET) film via sputtering magnetron ions (Fig. 6a).

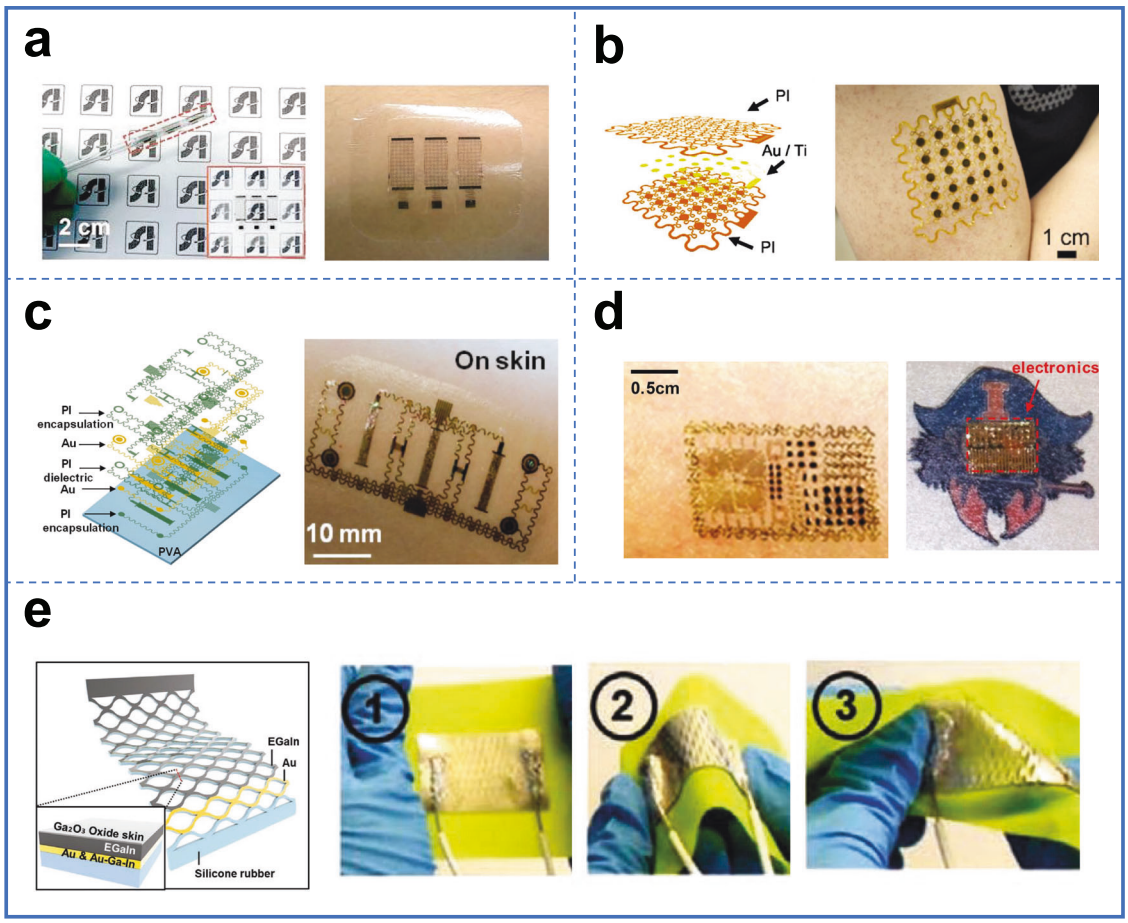

Fig. 6 Metal-based electrodes. a The fabrication steps of patterned microstructure-enhanced microelectrodes. **b** The reusable multichannel EMG sensor attached to the upper arm. **c** On-skin electrodes with serpentine design. **d** Epidermal electrode systems including EMG and ECG sensors. **e** The schematic illustration and the softness of the LM-eKE. **a** Reproduced with permission[106]. Copyright @ 2022, Wiley-VCH. **b** Reproduced with permission[107]. Copyright @ 2017, Springer Nature. **c** Reproduced with permission[104]. Copyright @ 2016, Wiley-VCH. **d** Reproduced with permission[22]. Copyright @ 2011, American Association for the Advancement of Science. **e** Reproduced with permission[110]. Copyright @ 2023, Wiley-VCH Verlag.

This deposition process allowed for the direct application of customized metal-patterned electrodes and various metal-patterned electrode arrays onto PET polymeric substrates without the need for high-temperature annealing or transfer processes. During a fist action, SNRs of the commercial gel electrodes, e-jet-printed metal electrodes, and e-jet-printed microstructure-enhanced electrodes were 20.136, 24.487, and 18.282 dB, respectively. EMG signal and SNR results confirm the effectiveness of electrohydrodynamic jet-printed metal electrodes, which produce comparable results to commercial gel electrodes. Likewise, Kim et al.[107] developed a large-area sEMG sensor array that covers multiple muscles by depositing and patterning metal electrodes (Ti/Au) on a PI film, which was then encapsulated with an additional layer of PI film for protection and stability (Fig. 6b). The multichannel sensor had a high average root mean square signals of 0.33 V and low noise of 0.032 V, which brought about a high SNR of 10.93 dB. Notably, the impedance of the prepared sEMG sensor was comparable with the Ag–AgCl electrode in the measurement frequency range from 10 Hz to 200 Hz. Xu et al.[104] designed an epidermal device based on thin metal films for high-quality sEMG signal acquisition (Fig. 6c). The electrodes consisted of a sputtered Au/Cr (5 nm/200 nm) bilayer and a silicon substrate. As a result, the thickness and Young's modulus of the overall device were about 60 μm and 60 kPa, respectively. The device's flexible design enables it to adhere to the skin through van der Waals interactions, providing comfort and freedom of motion without constraining natural skin movements. The incorporation of a low-modulus elastomer substrate enhances the softness of metal-based electrodes. These metal-based electrodes were widely utilized in diverse fields, including prosthetic control with sensory feedback, monitoring lower back exertion, and implementing electrical muscle stimulation with feedback control. In addition, reasonable structural designs can improve the flexibility and stretchability of metal-based electrodes as well. Kim et al.[22] prepared serpentine electrodes owning effective elastic moduli of 140 kPa via the microstructure design (Fig. 6d). When the loading strain reached 30%, the stress-strain curve of loading and unloading was a purely elastic response. At the same time, the maximum principal strain of electrodes was less than 0.2%. Recent research is devoted to human-computer interaction systems utilizing human physiological signal, which offers direct communication pathways between human and external electronic devices. The conventional electrodes for measuring electrophysiology should adhere to the skin by using pads or conductive gels. However, this way constrains natural skin deformation and even causes skin irritation and allergic reactions. In order to address those problems, Lee et al.[100] designed stretchable, skin-wearable, conformal Au electrodes for the acquisition of sEMG signals. A pair of electrodes by aligning with the submental muscles can record the swallowing sEMG signals required. As the electrode monitored the skin in real time during prolonged contacting, the electrode surface was inevitably contaminated by the skin oil, which caused a rise in the skin-electrode impedance and degradation of signal quality. He et al.[108] grafted poly(2-methacryloyloxyethyl phosphorylcholine) (PMPC) polymer brush onto the Au-coated PDMS electrode surface, the surface of which can be cleaned by water rinsing. Despite the SNR of PMPC-Au/PDMS electrode being reduced after contamination by skin oil, the SNR recovered after water rinsing, which demonstrated that electrode with an anti-epidermal-surface-lipid feature offers a perspective on developing next-generation flexible electronics.

Liquid metal (LM) refers to metallic materials that are in a liquid state at room temperature or relatively low temperatures. LM is widely acknowledged as an electrode material for monitoring electrophysiological signals due to its exceptional properties, including high deformability, conductivity, non-toxicity, and recyclability[81,109–114]. Gallium (Ga)-based LM alloys have gained significant popularity due to their exceptional metallic conductivity and inherent deformable properties. LM alloys, existing in a liquid state at ambient temperatures, possess the ability to conform effortlessly to the deformation of surrounding materials. The characteristic, coupled with their high conductivity, enables the creation of highly stretchable electrodes with minimal electromechanical coupling. Choi et al.[110] developed an LM-coated elastic kirigami electrode (LM-eKE) with remarkable mechanical deformability (up to 820% stretchability). ThisLM-eKE design combines high electrical conductivity with low electromechanical coupling (Fig. 6e). The LM-eKE comprises a kirigami-patterned silicone membrane that is coated with a thin layer of Au film and a layer of eutectic gallium-indium (EGaIn) LM alloy. The LM layer and Au film demonstrate superior wettability and material affinity, facilitating the formation of a solid–liquid biphasic film. The biphasic film of Au and EGaIn possesses minimal mechanical stiffness, enabling the LM-eKE to maintain a low elastic modulus (~kPa scale) while offering exceptional deformability. With its aforementioned characteristics, the LM-eKE demonstrates promising potential for applications in healthcare, robotics, and wearable devices. In order to prevent leakage of liquid metal during stretching, Lim et al.[113] prepared stretchable and highly conductive Ga-based bioelectronic devices encapsulated by a wrinkled Au/PEDOT layer. The Ga-based bioelectronic devices demonstrate remarkable flexibility and elasticity, with Young's modulus of 2 MPa at 3% stretching, while also exhibiting an electrical conductivity of 2×10^4 S m^{-1}. The Ga-based bioelectronic devices fabricated on a PDMS substrate, enable the measurement and analysis of EMG signals, demonstrating their precision and biostability. The flexible Ga-based bioelectronic devices exhibit conformability to curvilinear skin surfaces, allowing for the acquisition of uniform EMG signals with a high SNR of 14.6 dB. The main characteristics of metal-based sEMG electrodes are summarized in Table 1 (see refs. [24,26,57,58,89,92,106,108,115–131]).

Carbon-based electrodes. Besides the metallic electrode materials mentioned in the previous sheet, carbon-based materials can be used to reduce the skin-to-electronic contact impedance and improve flexibility, such as graphene, reduced graphene oxide (rGO), and CNTs[132–134]. In the past several decades, low-dimensional carbon materials with large contact areas and high conductivity for monitoring physiological signals have attracted great interest. Remarkably, CNT and graphene were found in 1991 and 2004, respectively.

CNT with flexibility and stability is a common carbon nanomaterial, which plays a vital part in monitoring physiological signals[46,102,135–138]. The electrode prepared by mixing CNTs and the conductive polymer is a better candidate for application as bioelectrical signal electrodes than the mixture of metal materials and conductive polymer, attributed to the random assembly properties of CNTs for better contact with the polymer. Lee et al.[46] mixed CNTs in adhesive PDMS to fabricate epidermis-like electronics for recording sEMG signals. The highly adhesive and conformal triangle electrode was designed based on the carbon nanotube/adhesive polydimethylsiloxane (CNTs/aPDMS) composite, which consisted of a PDMS substrate, an Au/Ti/PI layer, a PDMS frame layer, and an interfacial layer (Fig. 7a). The CNT electrode had a low modulus of 27.5 kPa with the addition of PDMS, which improved the measurement fidelity and conformal contact. As a result, the conductivity and contact impedance of CNT/aPDMS electrode was 16.4 S m^{-1} and 241 kV (40 Hz), respectively. Another approach to obtain skin-adhesive electronic electrodes was to disperse CNTs into the biocompatible and porous silk nanofibrous (SNF) networks. Kim and colleagues applied CNT ink by brush coating method uniformly dispersed on SNF and removed from the substrate to prepare the CNT/SNF e-tattoo[139]. The designed CNT/SNF e-tattoo combines the biocompatibility and porous nature of SNF with the high electrical conductivity of CNT, making the SNF film uniformly coated with

Table 1. Summary of metal-based sEMG electrodes.

Electrode material	Manufacturing method	Conductivity/resistivity	SNR/amplitude/contact impedance	Ref.
Au/UL-Sil/textile	Sputter deposition	——	5.00 mV	24
CuNW mesh	Solution-based nucleation and growth	——	80 dB	26
Au nanomesh/PVA	Electrospinning	5.30×10^{-7} Ω m	1 mV	57
Cu-PDMS	Femtosecond laser-activated metal deposition	3.75×10^{7} S m^{-1}	18.87 dB	58
Au/plasticized silk	Plasticization process	7 Ω sq^{-1}	17.17 dB	89
AgNWs/GEPC	Mask printing, transfer technique	9.66 Ω sq^{-1}	23.64 dB	92
Au/Cr-PET	Electrohydrodynamic jet printing	——	31.13 dB	106
PMPC-Au/PDMS	Deposition, surface-initiated atom transfer radical polymerization	2.75 Ω sq^{-1}	29 ± 2.30 dB	108
Ag-PTFE	Co-sputtering process	3.09–17.23 W sq^{-1}	——	115
Au nanoparticle	e-beam evaporation, electrodeposition	270 mW sq^{-1}	1.04 mV	116
Ti thin film	Glancing angle deposition	$1–15 \times 10^{-6}$ Ω m	——	117
AgNW-PDMS	Polyol method	5000 S cm^{-1}	24.70 dB	118
AgNWs/SEBS	Spray printing	11,000 S cm^{-1}	20.70 dB	119
TPU/hydrogel/Au	Thermally cured, mechanically interlocked	40.9 Ω sq^{-1}	43.03 dB	120
ECC-PDMS	Spin-coated	9.43×10^{-5} Ω cm	33.99 dB	121
Au/Cr	Thermal deposition	——	0.30 mV	122
ECC	Spin-coating	7.04×10^{5} Ω cm	4.66 dB	123
Au, Au/PU nanomesh	Electrospinning, magnetron sputtering	——	0.40 mV	124
PTFE/AgNWs/silk	Depositing, electrospinning	3.58 Ω sq^{-1}	22.59 dB	125
AgNW-TPE	Bubble blowing, spin-coating, transferring	2.98–155.50 Ω sq^{-1}	40 dB	126
Ti/Au	Laser-processed	——	0.40 mV	127
Cu–Au core–shell NW	Laser patterning process	——	22.17 dB	128
AgNW/Ecoflex	Dissolve, dry	25 S cm^{-1}	24.50 dB	129
Au	Deposition	——	21.09 dB	130
Ag-In-Ga-SIS	Print, heat pressing	7.02×10^{5} S m^{-1}	——	131

CNT material with single-sided conductive properties to avoid damage caused by direct contact between CNT and skin. The electrodes exhibited highly stable electrical properties and mechanical durability under tensile compressive, and torsional mechanical deformation conditions. In conclusion, the prepared CNT/SNF e-tattoo can test clear and without noise sEMG signals.

Nevertheless, CNT can be induced persistent inflammation and fibrosis attributed to its toxicity of CNT. Meanwhile, long-term inhalation of CNT can lead to lung cancer and genetic damage to the lungs. Besides one-dimensional (1D) CNT materials mentioned above, two-dimensional (2D) graphene is an electrode material attributed to outstanding mechanical, flexibility, biocompatibility, and electrical properties[140–143]. In order to obtain ultrathin and soft epidermal sensors, epidermal sensors made of graphene has been received a lot of attention from researchers. Ameri and co-workers fabricated a flexible and ultrathin graphene electronic tattoo (GET) via the "wet transfer, dry patterning" method[135]. The graphene was obtained using the atmospheric pressure chemical vapor deposition method. The ultrathin GET can stay attached to human skin and can withstand skin deformation for several hours for physiological measurements, such as ECG, EMG, and EEG. Specifically, the stretchability of ultrathin GET was more than 40%. When measuring sEMG signals, the tester squeezed a handgrip by using GET and gel electrodes (Fig. 7b). The result showed that the SNR and susceptibility to the motion of GET were comparable to that of gel electrodes. With advances in printing methods, wearable electronics are becoming more and more comfortable and flexible. The functionalized conductive graphene is gradually being used in domains such as wireless flexible circuits and recording of muscle activities, owing to its biocompatibility and solderability. Kwon et al.[144] prepared high-aspect ratio functionalized conductive graphene (FCG) electrodes by utilizing the all-printed, nanomembrane electronics (p-NHE) method. It is proven that the light and flexible FCG electrodes can be stretched up to 60% with highly conformal lamination on the skin. There was a negligible change in signal quality according to the acquisition of sEMG signals and SNR after 100 bending cycles. During extension and compression, the FCG electrode with highly conformal lamination on the human skin maintained contact quality (Fig. 7c). The porous electrode accelerated sweat evaporation to avoid perspiration accumulation between the devices and the skin. In addition, the transient CO_2 laser heating held great promise for converting polymer films into porous graphene. Sun and co-workers prepared stretchable porous graphene electrodes based on commercial PI films through CO_2 laser patterning, which can record high-quality sEMG signals from human skin[71] (Fig. 7d). The result indicated that the device had a low resistance of 10.96 Ω sq^{-1} and a great failure strain of 330%. Notably, the resistance of the porous graphene electrodes only boosted (~7%) at a bending radius of 2.5 mm after 500 cycles indicating the stretchable and mechanically compliant of the device. In addition, the porous graphene device owned good biocompatibility due to the electrode being attached to the skin for 7 days without inflammation. Therefore, the porous electrodes have remarkable capabilities in recording bioelectrical signals from the human skin. Previously reported electrophysiological sensors were created by using high-cost materials and complex processes. Not only that, using the above method only produced a few electrodes. According to this problem, Li et al.[145] prepared large-scale rGO electrodes by using simultaneous room-temperature reduction and patterning processes. Patterned Cu was sputtered on the silicon substrate and immersed in GO solution to generate rGO under the

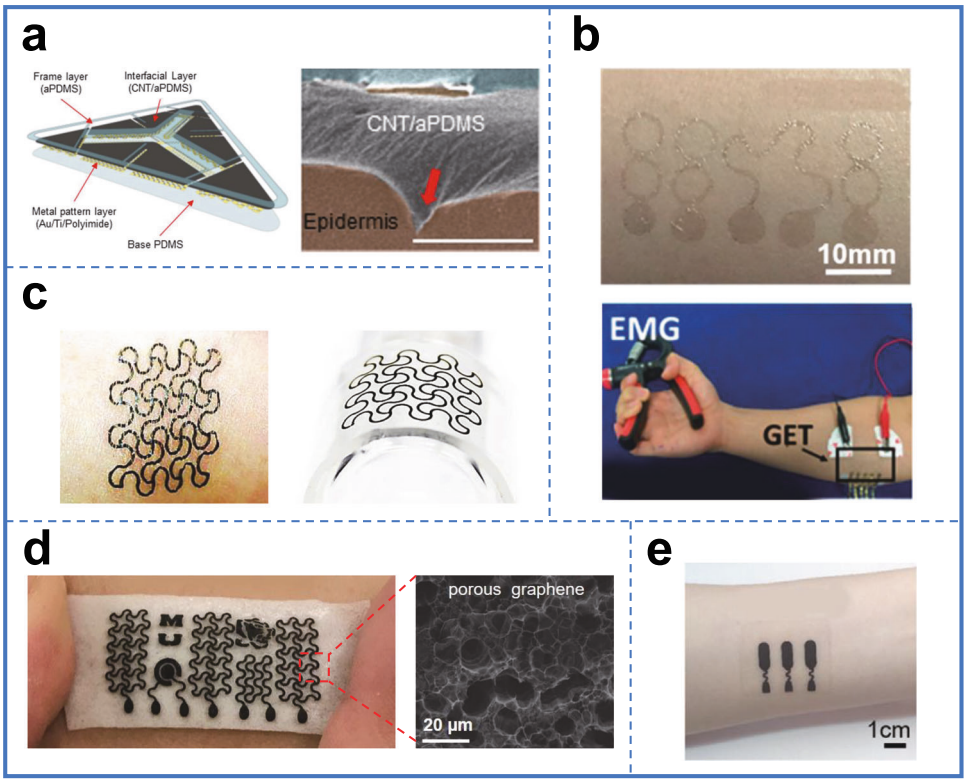

Fig. 7 Carbon-based electrodes. a The CNTs/PDMS composite electrode. **b** The GET attached to the skin. **c** The p-NHE adhering to the skin. **d** The gas-permeable, multifunctional on-skin bioelectronic sensing systems. **e** rGO-PDMS electrodes for monitoring sEMG signals. **a** Reproduced with permission[46]. Copyright @ 2014, Springer Nature. **b** Reproduced with permission[135]. Copyright @ 2017, American Chemical Society. **c** Reproduced with permission[144]. Copyright @ 2020, Springer Nature. **d** Reproduced with permission[71]. Copyright @ 2018, Wiley-VCH. **e** Reproduced with permission[145]. Copyright @ 2020, Elsevier.

Table 2. Summary of carbon-based sEMG electrodes.

Electrode material	Manufacturing method	Conductivity/resistivity	SNR/amplitude/contact impedance	Ref.
CNT/aPDMS	Dispersed mixing	16.4 S m^{-1}	241 kV (40 Hz)	46
Laser-induced porous graphene	Direct laser patterning	270 mW sq^{-1}	~17 kΩ (100 Hz)	71
CNT-TPU	Laser patterning, Heat	——	3.4×10^{-4}–1.4×10^{-7} Ω (100 Hz)	134
Graphene	Wet transfer, dry patterning	——	15.22 dB	135
CNT/SNF	Electrospinning	1.5×10^{-3} Ω m	——	139
FCG	AJP, Spin-coating, Photonicsintering	——	9.5 dB	144
rGO	Modified Hummers' method	——	16.8 dB	145
rGO–porous PDMS	Solution-based approach	1.5 kΩ sq^{-1}	——	146
Laser-induced graphene-PDMS	CO_2 laser processing technique	50 Ω sq^{-1}	——	147
Graphene-clad textile	Three-step coating approach	——	87.5 kΩ (10 Hz)	148
CB/CNT/SEBS	Electrospun	——	0.9 mV	149
Graphene	Laser	——	48.659 dB	150
graphene aqueous ink	Sonicate	——	10^5 (1 Hz)	151
PC/rGO/PVA hydrogel	Mixing	——	0.4 mV	152

room-temperature solution process. The low impedance of the rGO electrode was obtained by the low thickness of the rGO film and the good adhesion between rGO electrodes and human skin owing to the adhesive PDMS. The rGO electrodes attached to the skin can capture high-fidelity EMG, EOG, and EEG signals (Fig. 7e). As described above, it can illustrate that these electrodes are the central component of applications in healthcare and health science research. The main characteristics of carbon-based sEMG electrodes are summarized in Table 2 (see refs. [46,71,134,135,139,144–152]).

Conductive polymers-based electrodes. Conducting polymers have great promise for biosensing applications, owing to their sole properties such as lightweight, flexibility, and scalability[153]. Conducting polymers are frequently used as substrates or encapsulation layers of the metal-based device. Conducting polymers can not only alleviate the mechanical mismatch between hard metal materials and human skin but also protect the electrodes from corrosion in the physiological environment. Among the various conducting polymers, conductive PPy, PEDOT, and PEDOT:PSS are broadly used[154–156].

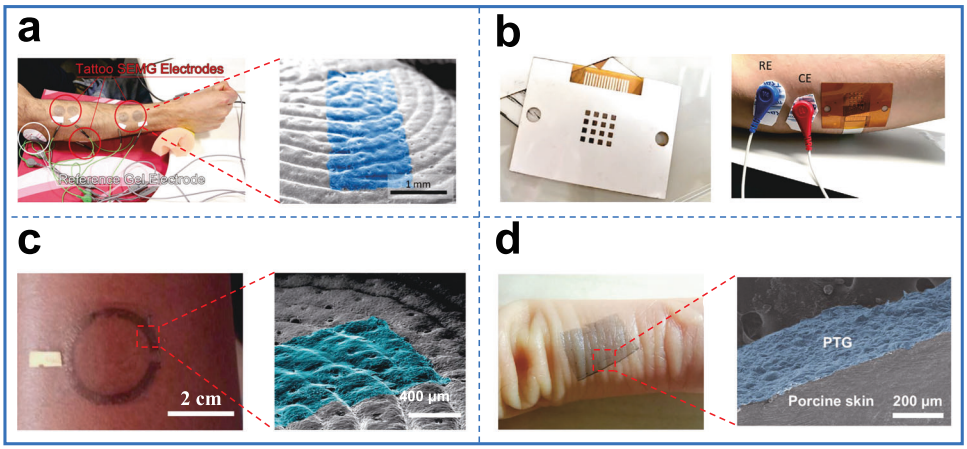

Fig. 8 Conductive polymers-based electrodes. a The photo and scanning electron microscope (SEM) image of tattoo nanosheet on human skin. **b** The photo of the electrode array before the peel-off of the top liner and attachment to the arm. **c** Assembled circular electrode transferred on the arm. **d** The PTG conformed on the human finger. **a** Reproduced with permission[157]. Copyright @ 2015, Wiley-VCH. **b** Reproduced with permission[158]. Copyright @ 2021, Springer Nature. **c** Reproduced with permission[159]. Copyright @ 2018, Wiley-VCH. **d** Reproduced with permission[160]. Copyright @ 2021, Springer Nature.

Zucca et al.[157] proposed a disposable tattoo electrode based on the PEDOT:PSS for recording sEMG signals. In detail, the conductive nanosheets were patterned by using PEDOT:PSS formulation. It is a remarkable fact that the tattoo nanosheet is a bilayer nanosheet constituted by ethylcellulose and PEDOT:PSS. A series of processes of fabrication, patterning, and transfer was shown in Fig. 8a. The decal transfer paper sheet was cured and blown with the compressed air gun. Afterward, the PEDOT:PSS dispersion was spin-coated. Finally, the tattoo nanosheet was freed from the transfer paper. Due to their good conductivity, ultra-conformability, and lightweight, conductive tattoo nanosheets are suitable for sEMG measurement. More importantly, electrodes were worn on the forearm for up to 12 h with no delamination or irritation to the skin. In 2021, Velasco-Bosom et al.[158] made flexible electrodes with digital fabrication techniques, which can capture high-quality sEMG signals. The electrode was fabricated through a series of operations (Fig. 8b). In detail, the ink printed silver tracks on a PI substrate. Subsequently, the device was deposited by PEDOT:PSS and then soak in saline. Finally, the top liner was removed to obtain the whole device. The volunteer was measured for sEMG signals through a 3-electrode configuration. Among them, the electrode was placed on the arm of the tester, whereas the Ag/AgCl electrodes were used as reference electrodes and counter electrodes, respectively. As a result, the impedance of the 4×4 array was about 2.7 MΩ at 60 Hz. As described above, the PEDOT:PSS electrode coated with ionic liquid gels had superb mechanical and electrical contact with skin. Unlike standard pre-gelled and dry electrodes, the tattoo electrode was thinner and had lower contact impedance. Thus, Ferrari prepared a patterned electrode with PEDOT:PSS directly inkjet-printed on tattoo paper[159]. The electrode had the advantages of stretchability (10%), ultrathin thickness (<1 μm), and long-term stability (48 h). The EMG and ECG signals recorded at different parts of the extremities and face confirmed the feasibility of electrophysiological detection of tattoo electrodes (Fig. 8c). The tattoo electrode had promising applications in diagnosis and therapy, brain–computer interface, and monitoring physical health in motion. Compared with the reported PEDOT:PSS electrode, the PEDOT:PSS-transferred CVD graphene film (PTG) prepared by Zhao et al.[160] has higher conductivity and SNR (23 ± 0.7 dB) for measuring sEMG signals. The ultrathin electrode had a low resistance of $24\,\Omega\,sq^{-1}$ and high electromechanical stability attributed to the synergistic effect between graphene and PEDOT:PSS (Fig. 8d). The PTG electrode with ultrathin property and high conductivity enabled accurate monitoring of electrophysiological signals, which can realize the facial nerve diseases diagnosis as well. The main characteristics of polymer-based sEMG electrodes are summarized in Table 3 (see refs. [9,29,55,73,76,82,83,97,115,153,157,159–169]).

Structural designs

The important thing for the measurement of sEMG signals is to design a superior structure of FNEs. The structural factors strongly affecting the acquired sEMG signal are the size, distance, and shape of the electrode. Therefore, while using FNEs for obtaining sEMG signals, the above-influencing factors are important to consider.

The FNEs with serpentine structures are inspired by spiderwebs. Rogers et al.[28] optimized various aspects of materials, device structure, operation and mounting, and fabrication methods. The prepared epidermal electronic system covering human skin can record large-area physiological information from the scalp and arm region. Each sensor consisted of 17 mesh electrodes with dimensions of $1\,cm \times 1\,cm$. The size of FNE arrays was $17\,cm \times 13\,cm$, which can cover the large-area region of the subject's back (Figs. 9a and 10). Recently, Hua et al.[170] fabricated a flexible and conformable matrix network e-skin for detecting temperature, ultraviolet light, and pressure simultaneously. The scanning electron microscope (SEM) images of FNEs are depicted in Fig. 9b. Wang et al.[171] reported soft, breathable FNEs with filamentary serpentines by using the cut-and-paste method, which can precisely capture sEMG signals and control prostheses. Especially the FNEs with 1.2-μm serpentine ribbons were permeable, conformable, and stretchable. In order to optimize the performance of the electrode, Rogers et al.[23] prepared different thicknesses, shapes, sizes, and spacing of the FNEs. It is known that conformal contact will be generated when the adhesion energy is larger than the sum of the bending and the elastic energy. Notably, the conformal contact also led to an increased SNR of bioelectrical signals. The FNEs exhibited the best mechanical properties when the device was in conformal contact with the skin at a thickness of 25 μm. In addition, the distance of FNEs was a crucial factor to influence the amplitude and crosstalk of bioelectrical signal. When FNEs were aligned with the muscle fibers and the electrode distance was 20 μm, high-quality signals, and minimal crosstalk were produced. Gandla et al.[95] prepared the frame-like sensor with serpentine structures via the ultrafast laser ablation technique, which is easy for attachment and detachment. The thicknesses and widths of the filamentary serpentine were 135 μm and 2.2 mm, respectively. The thicknesses and widths of the deformable electrodes were 25 μm and 0.4 mm, respectively. In order to realize the properties of flexibility and

Table 3. Summary of polymer-based sEMG electrodes.

Electrode material	Manufacturing method	Conductivity/resistivity	SNR/amplitude/contact impedance	Ref.
AHBH-ECC	Layer-by-layer pouring	——	29.2 ± 0.3 dB	9
PWS	Drop-casting	390 S cm^{-1}	82 KΩ (10 Hz)	29
PEDOT:PSS	Screen-printed	——	80.4 KΩ (10 Hz)	55
HP-AgNW/TPU	Breath figure method	7.9 Ω sq^{-1}	24.9 dB	73
HPAN/PU/AgNW	Electrospinning, vacuum filtration	——	25 dB	76
PEDOT:[$PSS_{(1)}$-b-$PPEGMEA_{(x)}$]	Reversible addition−fragmentation transfer process	2.14 S cm^{-1}	23.4 dB	82
TPU	Mechanical interlocking	40.9 ± 6.3 Ω sq^{-1}	43.03 dB	83
PEDOT:PSS/PVA	Mixing	2.0×10^{-5}–5.0×10^{-5} S cm^{-1}	29.50 ± 1.30 dB	97
PTFE-Ag	Co-sputtering process	3.09–17.23 W sq^{-1}	——	115
PEDOT:PSS	Inkjet-printed	240 ± 10 S cm^{-1}	26 ± 2 dB	153
Ethylcellulose/PEDOT:PSS	Decal transfer paper	8–70 S cm^{-1}	——	157
PEDOT:PSS	Inkjet-printed	——	300 KΩ (100 Hz)	159
PEDOT:PSS-transferred CVD graphene film	Spin-coating	24 Ω sq^{-1}	23 ± 0.7 dB	160
PEDOT:PSS	Glyceroand and polysorbate additive treatment	70–140 S cm^{-1}	35.23 ± 1.94 dB	161
PPy@AM-SF/CNC	In-situ polymerization	112.4 S m^{-1}	28 Ω	162
Supramolecular solvent/PEDOT:PSS/elastic polymer networks	Solution process	1–37 S cm^{-1}	6.25 Ω (10^2–10^4 Hz)	163
Poly(ionic liquid)	Spinning	0.50 mS cm^{-1}	——	164
PEDOT:PSS	Inkjet-printed	1000 S cm^{-1}	24.8 dB	165
SF organohydrogel	One-step, UV light illumination	——	27.8 Ω	166
PEDOT:PSS-PVA-tannic acid	Drop-casting	122 S cm^{-1}	256 KΩ (10 Hz)	167
PEDOT:PSS/AgNW/PEDOT:PSS	Spin-coating	——	50 KΩ (100 Hz)	168
Supramolecular polymer	Spray-coat	134 Ω sq^{-1}	41.8 KΩ (100 Hz)	169

stretchability, the structure of FNEs is designed to be a serpentine structure covering large-area human skin.

It is necessary to improve the comfort and safety of testers when using physiological monitoring electronics for a long period. Usually, the FNEs with porous structures have properties of high stretchability and breathability for conformally adhering to human skin. In addition, the porous structures FNEs reduce inflammation and irritation caused by prolonged skin adhesion. Therefore, to prepare epidermal electronic materials to achieve long-term wear resistance, it is imperative to develop breathable materials. To address this bottleneck in the development of these materials, Zhou et al.[73] proposed the preparation of epidermal electronic materials utilizing breath graphs and obtained ultrathin breathable electrodes with porous structure. The electrodes have good air permeability, allow sweat to evaporate freely, and their ultrathin properties (<10 microns) make them close to the skin, which improves the quality of monitoring biological signals. The conductive film was prepared by combining AgNWs with porous TPU via the simple and efficient breath figure method. The line width of FNEs with serpentine structure was 0.5 mm as shown in Fig. 9c. The porous structure of FNEs had evenly distributed through the SEM images. As a result, the ultrathin FNEs with the porous structure were capable to capture EMG and ECG signals by contacting the human skin.

Fractal geometry designs can be interpreted that small section pieces that are similar to the overall pattern. Compared with the serpentine patterns mentioned above, fractal designs can improve elastic strain according to the required dimensions and support multiple deformation modes. Fan et al.[172] prepared thin films with the fractal pattern, which can acquire higher quality impedance and SNR than conventional gel electrodes. The fractal FNEs with elastomers achieved elastic deformation. The first step of fabrication of the FNE array was coating and curing liquid PI on a Si wafer. And then, Cr and Au were generated by electron beam evaporation. Following patterning and etching, the encapsulated device was obtained through a photoresist mask and oxygen plasma etch (Fig. 9d).

Previous flexible extensible electronics were generally based on 2D designs (such as snake-shaped wires, partitioned wires, etc.), increasing the extensibility of devices by using in-plane design. These 2D designs can only achieve very high ductility without packaging. However, in the actual use situation, these devices need to be protected by some additional packaging. Only in this way can the device be protected from external damage in the actual application, and at the same time, the toxic parts of the implanted devices cannot cause toxicity to human tissues. However, with the addition of packaging materials, the scalability of previous 2D designs will be reduced. Therefore, Jang et al.[2] used a three-dimensional (3D) spiral design to replace the previous 2D serpentine structure. The 2D serpentine structure was selectively pasted onto a pre-stretched elastic base. While the base was released, the 2D serpentine structure wire was compressed and flexed into a 3D helix (Fig. 9e). Helix can still achieve more than 131% ductility in packaging. As for 2D structure, the extensibility in packaging was generally less than 10–20%, indicating that applications in many scenarios are limited.

PASSIVE ELECTRODE ARRAYS

sEMG signals are acquired with the main sources of interference being motion artifacts and industrial frequency interference. Motion artifacts are mainly caused by the relative movement between the skin surface position and the electrodes, while the industrial frequency interference is introduced by the high skin contact impedance of the electrodes and the poor contact between the

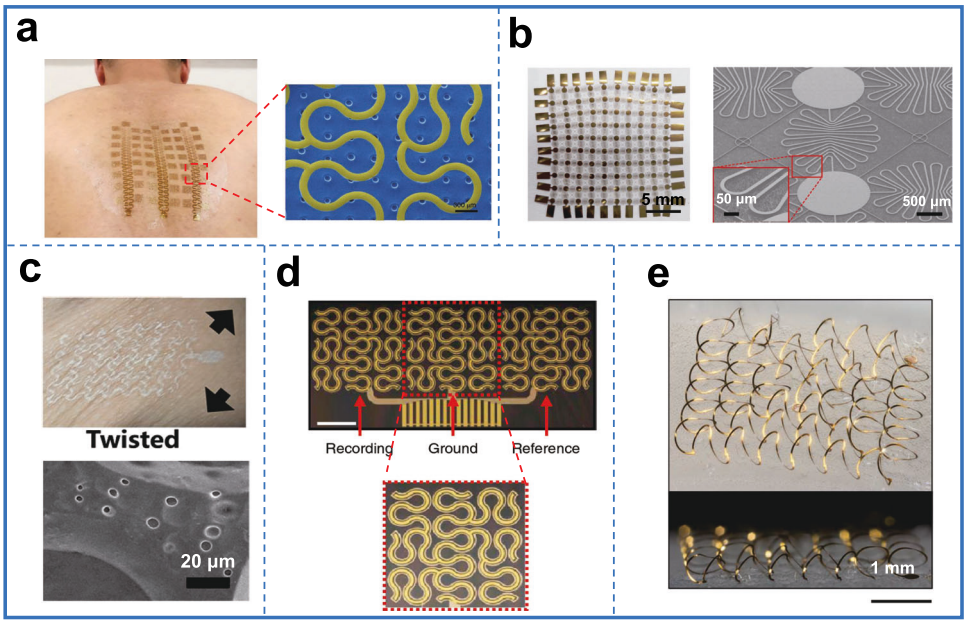

Fig. 9 The FNEs with different structures. a The photograph of large-area epidermal electrodes laminated on the back of a subject. **b** The optical image of the fabricated PI network. **c** The film electrode patterned into a filamentary serpentine structure. **d** The schematic image of the fractal design device mounted on skin. **e** The 2D serpentine structure wire is compressed and flexed into a 3D helix. **a** Reproduced with permission[28]. Copyright @ 2019, Springer Nature. **b** Reproduced with permission[170]. Copyright @ 2018, Springer Nature. **c** Reproduced with permission[73]. Copyright @ 2020, American Chemical Society. **d** Reproduced with permission[172]. Copyright @ 2014, Springer Nature. **e** Reproduced with permission[2]. Copyright @ 2014, Springer Nature.

high-input impedance of the amplifier and the electrodes and the skin. Although traditional passive sEMG electrodes can achieve painless measurement of EMG signals, they have technical defects such as poor reliability of sEMG signal transmission and low spatiotemporal resolution. With the development of passive FNEs designed towards the array, the FNEs achieve high spatiotemporal resolution. However, the increment in the number of passive FNEs arrays wires not only leads to signal crosstalk but also significantly decreases the SNR[17,107,121,135,170,173].

Typically, traditional single-channel FNEs with a reference electrode and a ground electrode is difficult to capture the sEMG signals from large-area human skin. The single channel can only measure a few muscle areas. Thus, multichannel sEMG arrays should be prepared to meet this requirement[174]. The measurement of biological signals by using passive arrays is shown in Fig. 10.

The inkjet printing technology is widely applied in the wearable devices field because it can realize large-area multifunction sensors with a simple and economical process[175,176]. In order to save cost and fast fabrication of electrode arrays, Roberts et al.[165] fabricated flexible multichannel PEDOT:PSS arrays by inkjet printing technology. Moreover, the inkjet printing method can provide the benefit of directly patterning electrodes on thin flexible films. The prepared multielectrode array consisted of a 4×7 electrode matrix on PI foil (Fig. 11a). The PEDOT:PSS multielectrode arrays can stick to the skin easily by humidifying it. The multielectrode arrays were simultaneously at any location on the skin for obtaining systematic sEMG signal data. Kwon et al.[52] prepared the L-EES through photolithography, wet/dry etching, metal deposition, and material transfer printing methods for the acquisition of high-quality sEMG signals. The total L-EES consisted of a 16-channel sEMG electrode array, a nanomembrane layer, an elastomer layer, and a fabric layer. As from Fig. 11b, the sEMG data was recorded by L-EES electrodes when the subject made five gestures. To realize the flexibility and multichannel of sEMG system, Alam et al.[60] have demonstrated the 12-channel system based on a flexible platform, which is attached to the skin to capture bioelectrical signals through copper electrodes and

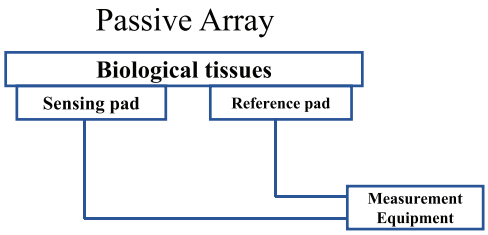

Fig. 10 The schematic diagram of passive electrodes for measuring sEMG signals.

transmit data through Bluetooth. Figure 11c shows the fabricated integrated FlexsEMG system owning ten extra electrodes. The sEMG signals were recorded from 12 channels at a 500 samples s^{-1} sampling rate, in which each sample was of 16 bits. With the development of ultrafast laser ablation techniques, electronic sensors can be large-area fabricated by this method at a lower cost. Gandla et al.[95] prepared a large-area frame-type sensor system to acquire sEMG signals from multiple muscles. The patch-based sensor with softness and breathability can conformally attach to human skin. It is verified that the sEMG signals from the movement of human muscles can control the robotic hand motion (Fig. 11d). Kim and co-workers also fabricated multichannel FNEs arrays by depositing and patterning the metal layers[107]. The total size of the prepared sensor web is 71 mm × 68 mm with a width of 1.2 mm frame, as shown in Fig. 11e. The multichannel 5×5 sEMG sensors can read signals from rugged regions on human skins by covering large areas, which was the biggest advantage of the multichannel sensor over the single-channel sensor.

ACTIVE ELECTRODE ARRAYS

To expand the test area of the sEMG signals, researchers increase the density of the sEMG signal. Nevertheless, the crosstalk of power lines becomes worse along with the increment of passive array electrode density. Simultaneously, the SNR is significantly

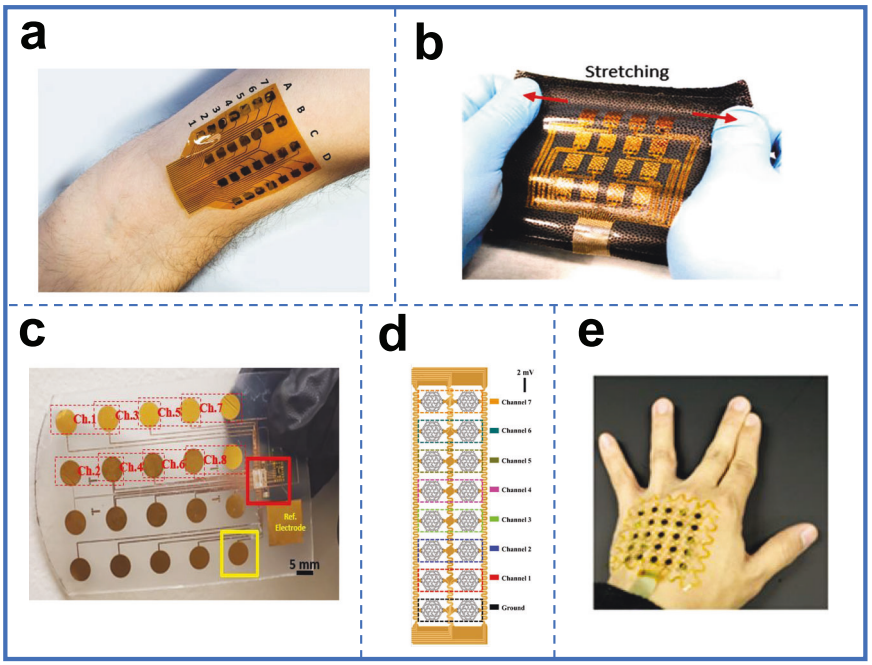

Fig. 11 Passive electrode arrays record sEMG signals. a The picture of the flexible multielectrode arrays sticking to the arm. **b** The schematic illustration of 16 channels of a single L-EES. **c** The picture of the fabricated FlexsEMG system. **d** The schematic of the sensor array with EMG electrode channels. **e** The optical picture of multichannel EMG electrode array. **a** Reproduced with permission[165]. Copyright @ 2016, Wiley-VCH. **b** Reproduced with permission[52]. Copyright @ 2020, Elsevier. **c** Reproduced with permission[60]. Copyright @ 2021, IEEE. **d** Reproduced with permission[95]. Copyright @ 2021, IEEE Industrial Electronics Society. **e** Reproduced with permission[107]. Copyright @ 2016, American Chemical Society.

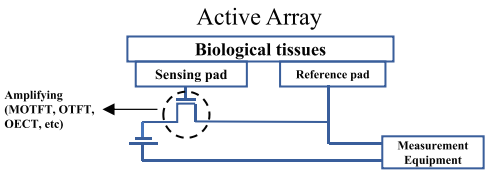

Fig. 12 Schematic diagram of active electrodes for measuring sEMG signals.

degraded due to the weak sEMG signals and electromagnetic waves susceptible to spatial[177–184]. In addition, the voltage amplitude of the electrophysiological signal in the human body is extremely weak. Therefore, the addition of active devices to passive electrode arrays is essential. Considering the design and fabrication of the electrode, the passive electrode is transformed into the active electrode by adding a signal conditioning circuit to the electrode. In general, the quality of sEMG signals can be improved by reducing the wire length between the electrode and the hardware acquisition system or by integrating the hardware acquisition module with the electrode. Amplification directly at the electrode position can reduce the industrial frequency interference caused by power lines. Passive electrode arrays are conventional designs that directly contact the skin, but their signal quality is susceptible to interference, including environmental noise and mutual electrode interference, resulting in a relatively low SNR. Active electrode arrays adopt more complex designs and circuit structures. By incorporating amplifiers, filters, and other circuits near the electrodes, active electrode arrays amplify and process bioelectric signals. This design reduces the influence of external noise on the signals and improves the SNR. Thereby, replacing flexible passive electrodes with flexible active electrodes in the measurement of bioelectrical signals has great prospects for development. Active electrodes are useful for the miniaturization and lightweight development of medical devices. The measurement of physiological signals by using active arrays is generally realized by transistors, which is shown in Fig. 12. The bioelectrical signal at the gate of the transistor is amplified to modulate the current between the source and the drain. Due to the addition of the active device requiring an additional power supply, the complexity of the electrodes and the uncertainty of signal acquisition increase. Thus, a comparative analysis is needed for the active and passive design of the electrodes. This section highlights the influence of different active layers of TFT.

TFT materials and device manufacturing

The TFT is an important basic device in the flexible electronics domain. In 1962, TFT was prepared by Weimer, which is a type of field-effect transistor amplifying analog and digital signals. A TFT consists of a substrate, an insulating dielectric layer, a semiconductor layer, a gate electrode, and the drain-source electrode. According to the order of each functional layer, the device structures can be classified into four categories:bottom gate top contact, bottom gate bottom contact, top gate bottom contact, and top gate top contact. Among them, the top gate top contact structure exhibits environmental stability owing to its semiconductor channel sealed by a dielectric layer to form a self-encapsulation. As regards bottom gate bottom contact structures, their carrier mobility is low due to high contact resistance and irregular dielectric surfaces. Compared to standard CMOS technology, TFT technology has advantages in compatibility with flexible electronics and circuits[185–187]. Owing to its low-power consumption, flexibility, and large surface area, TFT has received a lot of attention in low-power ICs, non-volatile memories, displays, and other fields[42,188,189]. The active layer affects the performance of the TFT, as an example, the number of charge carriers produced in the device operation can affect the saturation current. Hence, to fabricate high-performance devices, it is necessary to select appropriate active layers. According to the different active layers, we classify TFT devices into the following three categories: silicon-

based TFTs[190–192], organic TFTs[30,41,193–195], and metal oxide TFTs[196–200].

Silicon-based TFTs. In 1979, LeComber et al.[201] prepared amorphous silicon TFT. However, amorphous silicon TFT has been unable to meet the development of flexible electronic technology due to its low carrier mobility, small opening current, and low stability. Subsequently, Depp et al.[202] designed the polycrystalline silicon TFT in 1980, which has higher carrier mobility and better performance in high-frequency signal processing than that of amorphous silicon TFT. Nevertheless, the preparation of polycrystalline silicon TFT requires high cost and process complexity.

As described above, it is challenging that traditional silicon-based TFT is used in the field of flexible health care because of their stiffness, fragility, high cost, process complexity, and poor biocompatibility. In addition, the manufacturing process of silicon-based TFT is approaching its physical limit[203]. Active circuits based on conventional silicon-based TFT can achieve signal preprocessing and enhancement of the SNR of sEMG signals. However, silicon-based TFT with poor mechanical flexibility significantly reduces the wearable performance of electrodes[204,205]. As can be seen, the fabrication of flexible active electrodes with both high spatiotemporal resolution, noise resistance, and high integration still faces great challenges[204–210].

Organic TFTs. Organic TFTs (OTFT) is a device with organic small molecule film and conjugated polymers as the semiconductor layer. An OTFT is composed of five parts: an organic semiconductor layer, a dielectric layer, a source electrode, a drain electrode, and a gate electrode. In 1986, Tsumura et al. prepared the first OTFT—the polythiophene TFT, which can be applied to organic electronic circuits. The polythiophene TFT had a carrier mobility of 1×10^{-5} $cm^2 V^{-1} s^{-1}$ and a threshold voltage of −13 V, and a current switching ratio of 1×10^2–1×10^3. In the early days, OTFT exhibited low charge mobility and poor operating stability not meeting the requirements of practical applications. However, in the last decade, with the increasing comprehension of the transport mechanisms of organic semiconductors, more and more high-performance organic semiconductor materials have been prepared and discovered. Compared with silicon-based TFTs, newly developed OTFTs have attracted great attention from researchers, and have an extremely broad development prospect in the fields of flexible electronics, owing to their advantages of low cost, high integration, high mobility, good ductility, simple preparation process, good mechanical flexibility, and compatibility with various flexible substrates[186,211–217]. For example, Zhang et al.[218] prepared the high-mobility OTFT of pyrroloxypyrrolidone-4-thiophene polymers by hydrogen bonding side chain work. They introduced urea groups into the side chains of TFT, which led to a more ordered stacking between molecular chains, resulting in high mobility up to 13.1 $cm^2 V^{-1} s^{-1}$. OTFTs have a lot of advantages, such as low-temperature solution processing, biocompatibility, and mechanical flexibility, which is the candidate for flexible electronics.

According to the above description of the performance advantages of OTFT, OTFT includes Organic Electrochemical Transistors (OECTs) and Organic Field Effect Transistors (OFETs), which are widely used in physiological monitoring fields, and so on. OFET is defined as a three-terminal device, which uses an organic semiconductor to interact with the analyte. Indeed, the current flow between the source and drain could be controlled by the gate voltage for amplifying voltage or current. Similarly, OECT is a three-electrode device comprising a source, drain, and gate electrode. The doping state in semiconductor channel material can cause changes in the electrical conductivity of OECT.

The carrier mobility of conjugated polymers as a class of flexible organic semiconductor materials is comparable to that of polycrystalline silicon, but their stretchability is relatively poor and needs to be improved. Wang et al.[193] prepared an intrinsically stretchable polymer transistor array (ISPTA) with a transistor density of 347 transistors per square centimeter. That was the highest density of any reported flexible stretchable transistor array at that time. The ISPTA had outstanding charge-carrier mobility with only slight changes after 1000 cycles of 100% strain testing. Notably, the "conjugated polymer/elastomer phase separation induced elasticity" (CONPHINE) layer served as the semiconductor of the proposed ISPTA (Fig. 13a). Based on the above manufacturing process, the team has developed the first flexible integrated circuit components, such as stretchable haptic circuits of active arrays integrated with sensor arrays adhered to an individual's skin. This makes it possible to create promising stretchable flexible electronic devices. Molecular structure optimization, co-doping modification, and construction of nanowire/fiber network structures for conjugated polymers can significantly enhance flexibility, however, reduce carrier mobility. To address these issues, Wang et al. constructed strain-insensitive intrinsically stretchable transistor arrays merging patterned elastomer layers with tunable stiffness into the transistor structure[30]. They enhanced the stiffness of the local region (elastiff layer) by changing the cross-link density of the elastomer, thus reducing the strain in the active region of the device. This method was compatible with existing preparation processes and constructs arrays with device densities of 340 transistors per square centimeter. In order to obtain reliability and compatibility of the elastiff layer, the SEBS elastiff layer was patterned on top of the transistors by using the stencil printing method (Fig. 13b). The source, drain, gate electrodes and of the strain-insensitive intrinsically stretchable transistor were all prepared by spray coating the CNT solution. Xu et al.[219] explored the concept of polymer-based nanoconfinement for preparing semiconductor films with stretchability. The used CONPHINE method can maintain mobility during stretching by improving chain dynamics and reducing embedded crystallinity. This method will advance the development of stretchable semiconductors for stretchable electronic skin applications.

Dianthra[2,3-b:2′,3′-f]thieno[3,2-b]thiophene (DNTT) OTFTs have electrical properties[197], good flexibility[220], and air stability[221], which provide the ideal material for monitoring physiological signals. In 2016, Someya et al.[41] demonstrated the OTFT on a flexible polyethylenenaphthalate (PEN) film, which comprised an Al gate, self-assembled monolayer gate dielectric, DNTT semiconductor, Au source, and Au drain (Fig. 13c). The admittance of the gel electrode formed by a CNT sheet and an aqueous hydrogel was 100 mS cm^{-2}. After amplification, the input SNR goes from 0.53 dB to 64 dB. Meanwhile, the gain of the amplifier exceeds 10 at a frequency below 1 kHz and 100 at a frequency below 100 Hz. Meaningfully, this work was the first time to integrate an active-matrix amplifier array with biocompatible gels for successfully amplifying bioelectrical signals. In 2019, Sugiyama et al.[194] designed a flexible organic amplifier based on OTFTs for recording weak bioelectrical signals. The circuit was made up of p-type OTFTs and thin-film capacitors consisting of parylene dielectrics, Al, and Au electrodes (Fig. 13d). The common-mode noise attenuation factor of the circuit was less than −12 dB. It is shown that the OTFTs and capacitors placed between ultra-flexible layers can improve the flexibility and stability of the device. Notably, DNTT served as the high-mobility semiconductor of the OTFTs. Similarly, Fuketa et al.[196] designed the OTFT with an organic semiconductor of DNTT for measuring sEMG signals. To achieve the property of ultra-flexibility, the OTFT was fabricated on a 1 mm-thick PEN film. Lee et al.[195] fabricated the flexible OECT-OFET electrode array, in which each detection cell consisted of an OECT and an OFET. The integration of OECTs and OFETs was made possible by choosing the OECT annealing temperature as low as 55 °C. The schematic cross-section of the whole electrode array is demonstrated in Fig. 13e.

Metal oxide TFTs. Amorphous silicon (a-Si) TFT and OTFT serve as amplifiers with high SNR and common-mode rejection ratio

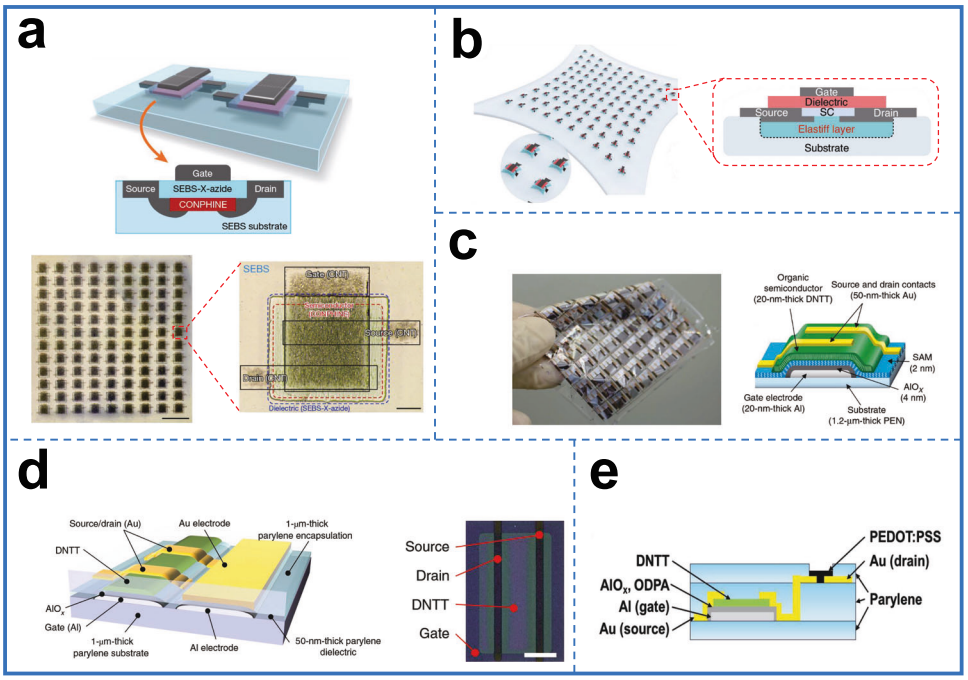

Fig. 13 Organic TFTs. a The schematic, optical microscopic image, and magnified image of the intrinsically stretchable OTFT. The Scale bar is 1 mm. **b** The schematic of the stretchable OTFT while stretching. **c** The picture and cross-sectional image of the OTFT on the PEN substrate. **d** The cross-sectional picture and a magnified view of an amplifier circuit with an OTFT. **e** The structure of the integrated device. **a** Reproduced with permission[193]. Copyright @ 2018, Springer Nature. **b** Reproduced with permission[30]. Copyright @ 2021, Springer Nature. **c** Reproduced with permission[41]. Copyright @ 2016, Springer Nature. **d** Reproduced with permission[194]. Copyright @ 2019, Springer Nature. **e** Reproduced with permission[195]. Copyright @ 2016, Wiley-VCH.

(CMRR), enabling to detection of weak bioelectrical signals. Nevertheless, attributed to their poor driving capability, they have high-power consumption and slow speed. In recent years, good results have been achieved in the research of oxide TFTs. Metal oxide TFTs (MOTFTs) not only have higher saturation mobility, but also have simpler production processes, lower input costs, and, especially for amorphous metal oxides, better performance consistency in mass-produced devices. Due to these advantages, MOTFTs have great potential for development and are therefore highly sought after. At present, MOTFTs with high mobility are used to prepare preamplifiers.

Although ZnO is considered to be the most promising material for TFT, the mobility of ZnO TFT is less than $10\,cm^2\,V^{-1}\,s^{-1}$ not enough for flexible electronics. After Nomura et al. reported that MOTFTs have high mobility in the amorphous state when the outermost electron of the metal element cation satisfies (n-1) $d^{10}ns^0$ $(n >= 4)$, different metal oxides and the doping of ZnO with some other elements have been investigated to improve the electrical properties of TFTs[222]. From a large number of research and experimental data, it can be concluded that the doping of In elements in ZnO increases the carrier concentration in the material and substantially improves the mobility of TFTs. To date, the indium gallium zinc oxide (IGZO) is a typical representative of MOTFT, which has high field-effect mobility and good stability[223]. Owing to the properties of flexibility, lightweight, and low cost, the IGZO TFTs are fabricated on large-area substrates for building wearable bioelectrical signal acquisition systems. Even though flexible unipolar IGZO analog circuits can achieve excellent performance, the circuit with low-power consumption and high gain should use both n-type and p-type TFTs.

There are many methods to prepare IGZO thin films, such as magnetron sputtering, sol-gel, chemical vapor deposition, atomic layer deposition, etc. Petti et al.[224] reported a flexible complementary amplifier consisting of p-type single-walled carbon nanotubes (SWCNTs) and an n-type IGZO TFT. The amplifiers were made on a 50 μm-thick PI foil by using a 6-mask process at a maximum temperature of 150 °C. The schematic cross-section of the amplifier and the photograph of the substrate are shown in Fig. 14a. In p-type TFT, the Al_2O_3 gate dielectric was prepared by atomic layer deposition, and the SWCNTs semiconductors layer was spray coated through a shadow mask. The DC gain of the complementary amplifier increased from 3.5 V/V to 27.2 V/V owing to the n-type TFT and a p-type TFT enabling the selection of the appropriate bias voltages of the circuit. Zulqarnain et al.[225] proposed a flexible patch implemented on foil with double gate self-aligned IGZO TFTs for acquiring and amplifying the ECG signals (Fig. 14b). Similarly, our group also fabricated a 16-channel FNEs system using IGZO TFTs for collecting sEMG signals[226]. The gate layer of the IGZO TFT has deposited molybdenum and indium–tin oxide. The source/drain contacts were connected to the IGZO semiconductor via dry etching (Fig. 14c). As a result, the SNR of the passive FNEs array and active FNEs array was 24.7 dB and 35.4 dB, respectively. In 2020, Yu et al. prepared 3D nanofiber network (FN) films through the blow-spinning technique. The 3D FN films included IGZO semiconductors, copper oxide, conducting indium–tin oxide, and copper metal[227]. According to the good flexibility of IGZO FN-based TFT, it had basically no degradation in performance after being bent 1000 times. IGZO FNs were deposited on the substrate as dielectric/gate contact via the blow-spinning method. Subsequently, the Al source/drain electrodes were prepared through thermal evaporation. The flexible IGZO FN-based TFTs were prepared on light and ultrathin PI substrates (Fig. 14d). To illustrate the amplification role of TFTs for biomedical applications, we describe the amplification circuits in "Analog circuits based on TFTs" in detail.

Analog circuits based on TFTs

In this section, progressive analog circuits based on TFTs are demonstrated. Signal amplification is the most basic analog signal

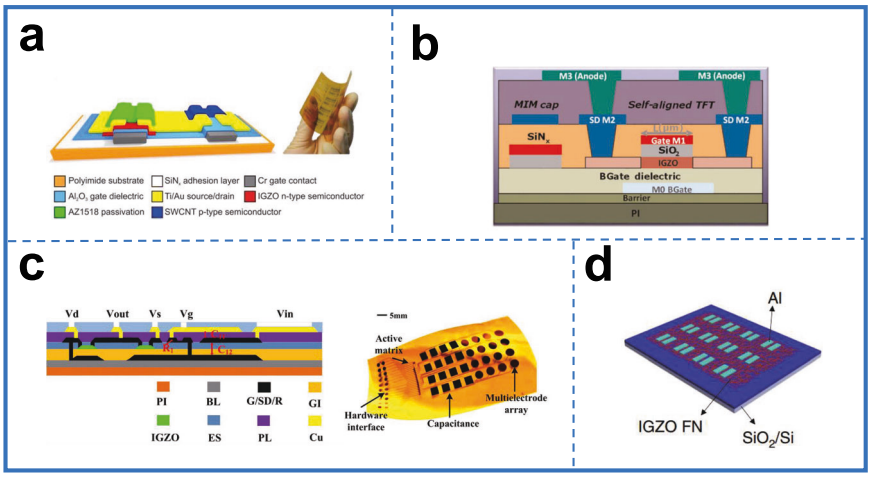

Fig. 14 Metal oxide TFTs. a The schematic cross-section of the complementary amplifier based on n-type IGZO and p-type SWCNT TFTs. **b** The cross-sectional view of TFT. **c** The structure of the integrated device and photograph of a sensor array. **d** The diagram of the IGZO TFT array. **a** Reproduced with permission[224]. Copyright @ 2017, Institute of Electrical and Electronics Engineers Inc. **b** Reproduced with permission[225]. Copyright @ 2020, Springer Nature. **c** Reproduced with permission[226]. Copyright @ 2020, Institute of Electrical and Electronics Engineers Inc. **d** Reproduced with permission[227]. Copyright @ 2020, Springer Nature.

processing function, which is realized by amplifying the electrical signal to the required amplitude through the amplification circuit. The performance index of the amplifier circuit is used to quantitatively describe the standard of the ground performance of the amplifier circuit and determine its scope of application. The gain (A_v) is the key parameter of amplifiers. A_v, often referred to as the magnification factor is a critical parameter of the amplification capability directly. A_v can be expressed as follows:

$$A_v = \frac{V_{out}}{V_{in}},$$

V_{out} and V_{in} is the output and the input voltage of the amplifier, respectively. As usual, A_v is expressed using a logarithmic scale, which is given by:

$$A_{v(dB)} = 20\log_{10}\left(\frac{V_{out}}{V_{in}}\right)$$

Bandwidth is another important amplifier indicator, which usually refers to the frequency difference between two half-power points with corresponding high and low-amplitude frequencies.

The sEMG signals sensed by the sEMG electrodes are low voltage (μV–mV), low frequency, weak bioelectrical signals, which need to be to be amplified, and thus the requirement for low-noise amplification gain is much higher than that of general non-amplifiers for non-biological signals. Therefore, in designing the myoelectric signal amplifier circuit, high A_v and high SNR are focused on. The unipolar circuit is the basic and most widely used amplifier circuit. Furthermore, some research is devoted to complementary circuits with an n-type TFT and a p-type TFT. This section will focus on unipolar circuits and complementary circuits.

Unipolar circuits. Mao et al.[226] prepared the 16-channel FNE array via the full lithography method. The reported amplifier circuit consisted of an amorphous IGZO TFT (a-IGZO TFT) as diode resistance and an a-IGZO TFT as driving resistance, respectively, which can largely amplify the sEMG signal. The high-gain measurements for input signal frequencies between 0 and 1000 Hz are shown in Fig. 15a, in which the frequency of 480 Hz matches the sEMG frequency band of 10–300 Hz. Particularly, the SNR of passive FNE and active FNE for sEMG signal acquisition system was 24.7 dB and 35.4 dB, respectively. The active FNE array with the amplification circuit enabled the enhancement of the bioelectrical signal quality, which is important for the recognition of muscle movements. In addition to MOTFT for building unipolar amplifier circuits, OTFT can be used in unipolar amplifier circuits due to its flexibility and low cost as well[228]. The OTFT was contained with $HfZrO_x$ (HZO) gating to prepare the amplifier circuit (Fig. 15b). Owing to the steep switching in sub-thermionic OTFTs, the high A_v is of 4.1×10^3 and 1.1×10^4 while operating voltages of −1 V and −3 V, respectively. The reported high gain under low operating voltage indicates that the built unipolar amplifier circuits based on sub-thermionic OTFTs have significant implications for the physiological signal monitoring area.

In addition to the above circuits, differential circuits of the amplifier can achieve higher gain. Most of the traditional amplifiers have a single-ended structure, which is difficult to distinguish the biological signal from the interference noise and monitor the physiological electrical signal under the low-noise condition. However, a differential amplifier is a circuit that measures signals that eliminate noise components. Sekitani's team has successfully developed the thinnest and lightest differential amplifier for biological instruments[194]. This slim, flexible organic differential amplifier accurately monitors weak biological signals at low-noise levels without any discomfort caused by the device attached to the body. Compared with the traditional single-end amplifier, the flexible differential amplifier developed in this study not only amplifies very weak bioelectric signals but also reduces the interference noise (Fig. 15c). As a result, the common-mode noise attenuation of the differential amplifier was less than −12 dB at a frequency of 1 kHz. When reducing the channel length of the OTFT from 50 μm to 10 μm, the bandwidth and the CMRR of the amplifier climbed up to 1.6 kHz and 44 dB at 50 Hz, respectively.

Owing to unipolar circuits suffering from high-power consumption, the traditional unipolar circuits only with n- or p-type TFT can't meet the current requirements for circuit performance. To solve this problem, the pseudo-CMOS design was employed, which uses only n- or p-type TFT for realizing the needed performance equal to complementary-type logic circuits. The advantages of the pseudo-CMOS design are as follows: (i) operating under a low-power supply. (ii) suitable for both enhanced- and depletion-mode TFTs. (iii) better noise tolerance[229]. In vivo, electronic monitoring systems help us understand the biological activity within the living body and are promising next-generation medical electronics. However, the currently used devices do not have good stability in vivo and are not very sensitive to biological signals. In order to

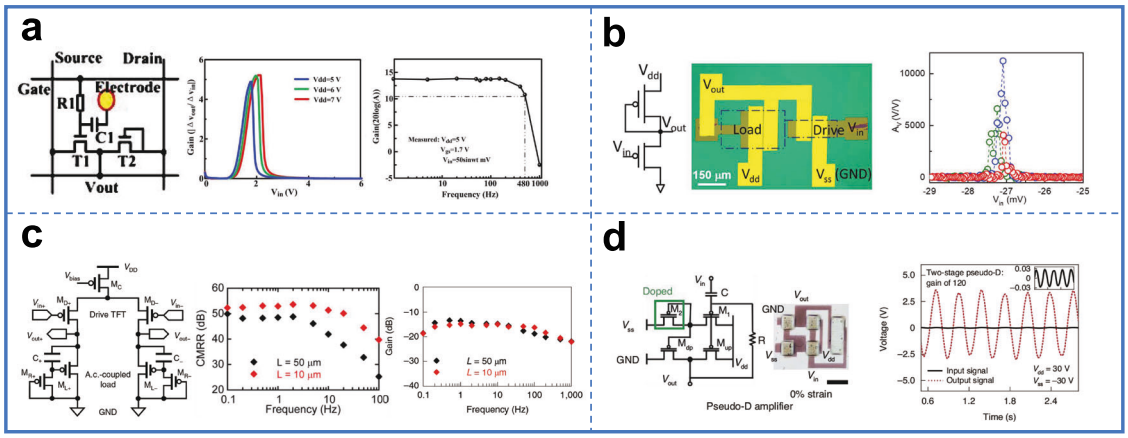

Fig. 15 Amplifier with unipolar circuits. a The circuit schematic and properties of the FNE array. **b** The circuit diagram of the amplifier based on sub-thermionic OTFTs. **c** Organic differential amplifier and its electrical performance. **d** Strain-insensitive digital and analog circuits for human electrophysiological signal conditioning. **a** Reproduced with permission[226]. Copyright @ 2020, Institute of Electrical and Electronics Engineers Inc. **b** Reproduced with permission[228]. Copyright @ 2021, Springer Nature. **c** Reproduced with permission[194]. Copyright @ 2019, Springer Nature. **d** Reproduced with permission[30]. Copyright @ 2021, Springer Nature.

obtain good mechanical flexibility, Bao's group developed a preparation process that achieves high yields and uniform device performance for different intrinsically stretchable materials[193]. To achieve the amplification of raw detected physiological signals on the skin, an amplifier was fabricated using a self-feedback design. The amplifier is combined with a stretchable pulse sensor to amplify the raw detected physiological signal. This work successfully develops a preparation process for organic materials and uses it to produce stretchable transistor arrays with signal processing and computational functions. Subsequently, Bao's group constructed integrated circuits based on this strain-insensitive transistor array that can be used for quantitative signal processing. In order to get the amplified sEMG signals, the output terminal of the electrodes was connected to the ground and input terminal of the pseudo-D amplifier, respectively[30]. From the sEMG signal, if there is no amplifier, the sEMG signal is masked by background noise. In contrast, when the stretchable amplifier is fitted to the human biceps, a significant EMG signal can be observed with approximately seven times the amplitude. Connecting two amplifiers in a series can even provide a total A_v of greater than 120 (Fig. 15d). The pseudo-CMOS D-type architecture of the amplifier design exhibits high gain and records weak bioelectrical signals. Because of the low cost and flexibility of carbon-based materials and devices, research on carbon-based materials is becoming increasingly abundant.

Complementary circuits. The unipolar circuit discussed in the previous section can be regarded as a general circuit. It consists of an n-type drive TFT and a load device that can act as a non-linear resistor. The load device can be a resistor, either an n-type TFT or a pseudo-CMOS TFT. This section discusses an amplifier circuit operating in complementary mode, which consists of an n-type TFT and a p-type TFT. Compared with unipolar circuits, complementary circuits have steady-state power consumption, which can be ignored except for the small power consumption caused by leakage current.

Petti et al.[224] also prepared a gain-tunable amplifier consisting of an n-type IGZO TFT and a p-type SWCNT TFT (Fig. 16a). The A_v of the amplifier can reach 28.7 dB by regulating the gate bias voltage of the SWCNT TFT, which is higher than that of unipolar amplifiers. Similarly, Jang's group manufactured the low-temperature polysilicon oxide (LTPO) TFTs constituted by p-type polysilicon (LTPS) TFT and n-type a-IGZO TFT by using six photomask steps[230]. As a result, the LTPO TFTs own an outstanding A_v of 264.5 V/V and a noise margin of 4.29 V, respectively. Likewise, Kim et al.[231] prepared the inverter assembled by the LTPS TFT and the a-IGZO TFT, which indicated the A_v of 114.28 V/V. In 2021, Yang et al.[232] fabricated printable OECT-based complementary voltage amplifiers, which can perform a series of processing of the signal, such as recording, amplifying, and filtering the bioelectrical signals. According to the previous introduction, the OECT with large transconductance values is ideal for recording weak signals. This work demonstrated complementary voltage amplifiers consisting of p-type and n-type enhancement-mode OECTs. The voltage gain dependence on the amplitude of the input signals is depicted in Fig. 16b. The highest gain is 30.4 dB with a 200 μV input signal, which indicated that the circuit still had great magnification capability at low frequency. In conclusion, the OECT-based complementary circuits can be widely applicable for amplifying low-amplitude voltage signals in electrophysiological signal recordings and electronic neural interfaces. Jeon et al.[233] proposed a two-stage amplifier with high gain for detecting bioelectrical signals prepared by LTPO technology. The proposed circuit with the Corbino structure is composed of LTPO TFTs. In addition, the second amplifier enhances the total voltage gain. Consequently, the average voltage gain (60.6 dB) of the whole circuit can be calculated from the data in Fig. 16c. Rahaman et al.[234] established the circuit with the two-stage LTPO operational amplifier (Fig. 16d). The operational amplifier consists of six p-type TFTs (T1, T3, T5, T6, T10, and T12) and seven n-type TFTs (T2, T4, T7–T9, T11, and T13). The first stage includes the input port, current mirror, and differential to the single-ended converter stage. The frequency and phase response of the prepared operational amplifier is displayed. The second stage is severed as an output buffer. It is indicated that the A_v of the amplifier starts from 50.7 dB and then falls to −3 dB from 10 Hz to 200 kHz. Notably, the maximum field-effect mobility of the p-type TFT and the n-type a-IGZO TFT was 80 $cm^2 V^{-1} s^{-1}$ and 11.5 $cm^2 V^{-1} s^{-1}$, respectively.

APPLICATIONS

As mentioned above, FNEs have played a cardinal role in flexible electronics. FNEs being in contact with the human skin have traced sEMG signals for analyzing human activities (such as facial expressions and body motion) and controlling external devices. Thus, this section focuses on the recent development of FNEs for human healthcare and HMI.

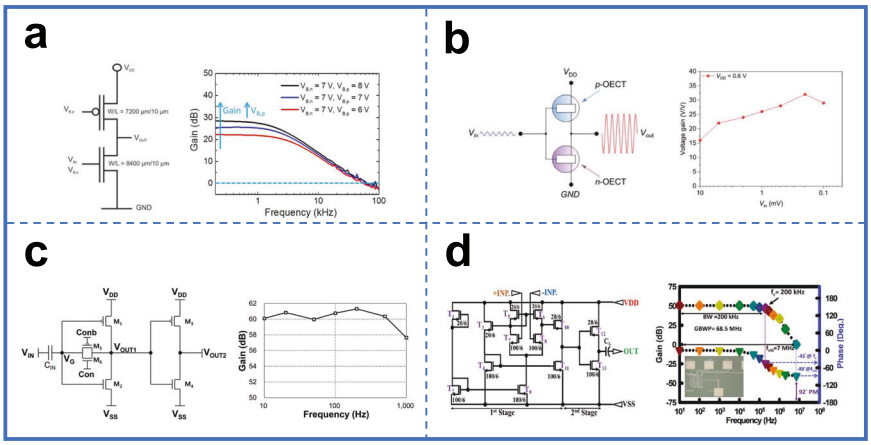

Fig. 16 Amplifier with hybrid-CMOS circuits. a The circuit schematic of the CS amplifier. **b** The circuit schematic of the low-noise neural signal amplifier, **c** the schematic diagram of the differential switched-capacitor amplifier stage, **d** the circuit schematic of the LTPO operational amplifier. a Reproduced with permission[224]. Copyright @ 2017, Institute of Electrical and Electronics Engineers Inc. **b** Reproduced with permission[232]. Copyright @ 2021, Wiley-VCH Verlag. **c** Reproduced with permission[233]. Copyright @ 2022, TAYLOR & FRANCIS LTD. d Reproduced with permission[234]. Copyright @ 2020, Institute of Electrical and Electronics Engineers Inc.

Healthcare

Analyzing sEMG signals is an effective method for diagnosis, therapy, and monitoring of human health. FNEs with ultra-thinness, low modulus, and high flexibility conformally attached to the skin could provide a chance for human healthcare. Lo et al.[55] prepared an elastic sponge electrode for recording high-quality bioelectrical signals, which reduced the contact impedance between the electrode and human skin and promoted the SNR of bioelectrical signals. The sponge electrodes can not only measure sEMG signals from skeletal muscle cells but also record weak EMG from smooth muscle cells. For instance, the non-invasive sponge electrodes can acquire high-quality signals from the abdominal surface of pregnant women, which can diagnose various risks, such as preterm labor (Fig. 17a). In addition, sEMG can also provide useful information for other diseases, such as assessing muscle fatigue, studying muscle pain and swallowing therapy, etc. Kim et al.[235] prepared a wireless flexible device for remote monitoring of dysphagia, which consists of honeycomb networks and a strain gauge. A sensor patch was placed in the submental area to keep the sEMG electrodes in contact with the skin (Fig. 17b). As a result, the impedance between the patch and human skin is lower than that of commercial electrodes. In addition, the sEMG signal datums measured by the electrode were plotted as circular graphs. Through comparing the circular graphs, the submental muscle activity under various conditions was easily captured. It was shown that in comparison to normal swallows, the datums recorded from effortful swallows were larger because of muscle movements by a large margin. Notably, the signal through the Mendelsohn maneuver exhibited an altitude increment of 200% and duration enhancement of 270% compared to that by normal swallows. The device was equipped to accurately monitor the swallowing disorder. Overall, the sEMG datum could provide clinically useful information and feedback during swallowing rehabilitation therapy. Farina et al.[236] demonstrated a neural interface following targeted muscle reinnervation to extract the sources of neural information. After decoding, the neural information was mapped into commands for potential prosthetic control. In detail, the sensors placed on the skin surface can capture the nerve signals from the spinal cord. The volunteer, after a certain period of learning, only needs to simulate moving the arm and doing different movements in his mind through motor imagination. Accordingly, the sensors on the prosthesis can receive the motor nerve electrical signals from the spine and analyze them, and then instruct the robot arm to complete multidegree of freedom movements (elbow and wrist joints), which can achieve most of the basic functions of a real arm (Fig. 17c). This technology focuses research on brain-machine interfaces on the nerves rather than the muscles, meaning that the use of spinal cord motor nerve signal sensing can more accurately represent the patient's motor awareness and can allow mechanical prostheses to be used with closer to intuitive control, which is certainly good news for people with disabilities.

Despite the high demand for FNEs in human health, there are still obvious problems with research in flexible electronics. This is mainly due to the limited accuracy of equipment acquisition and the need to improve diagnostic expertise. Therefore, the breakthrough of FNEs lies in improving signal acquisition precision, comfortable feeling during wearing, and algorithms.

Human–machine interfaces

From the above analysis, we know the acquired sEMG signals are directly associated with states of human motion. sEMG signals acquired from the human arm can control external devices. Therefore, sEMG signals can be applied in HMI through processing related to human motion[122]. The utilization of sEMG as control signals and skin-based current stimulation as feedback in human–machine interfaces presents a significant medical application in the fields of robotics, prosthetics, and machine-assisted living.

Inzelberg et al.[237] demonstrated a facial sEMG system, which can capture different muscles associated with distinct smiles for providing precise physiological information. It is shown that the differential sEMG data segment was mapped by different complex facial expressions of the subjects in 20 s during a conversation with other people (Fig. 18a). The sEMG system consisted of eight electrodes adhered to the volunteer's cheek. Kwon et al.[144] reported wireless, multilayer, and flexible electronic systems by using a functional material additive nanofabrication technique. The all-printed electronics with machine learning can provide different types of universal human–machine interfaces. The flexible system can control external targets in real time for daily life by utilizing measured EMG data. For example, the device-enabled EMG and *z* axis acceleration can control external devices, such as a quadcopter drone and RC car (Fig. 18b). In a word, the all-printed electronics have great potential for a serial of portable HMI applications, such as control of a humanoid robot, drone, prosthetic hand, etc. Guo et al.[123] fabricated electronic systems with a series of highly conductive electrodes, which can not only monitor electrophysiological but also be used for HMI

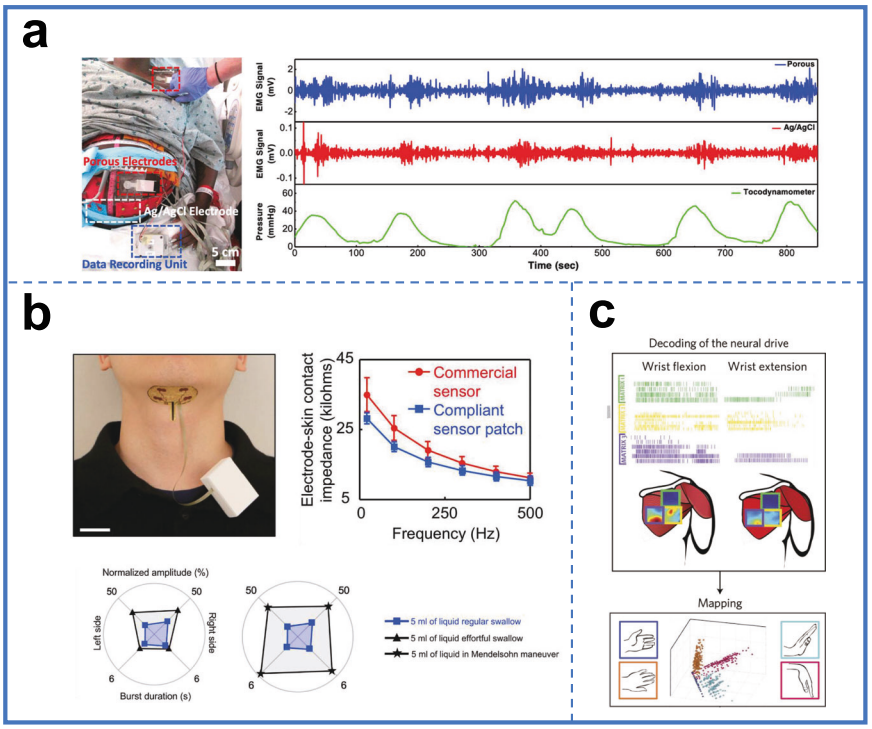

Fig. 17 The electrode arrays play a role in health monitoring. a The EMG signal recording from uterine contraction activities in a clinical setting. **b** The sensor patch with remote control unit can study a patient diagnosed with Parkinson's disease and dysphagia. **c** The discharge timings of the innervating motor neurons are decoded by deconvolution of the sEMG signals. **a** Reproduced with permission[55]. Copyright @ 2022, American Chemical Society. **b** Reproduced with permission[235]. Copyright @ 2019, AAAS. **c** Reproduced with permission[236]. Copyright @ 2017, Springer Nature.

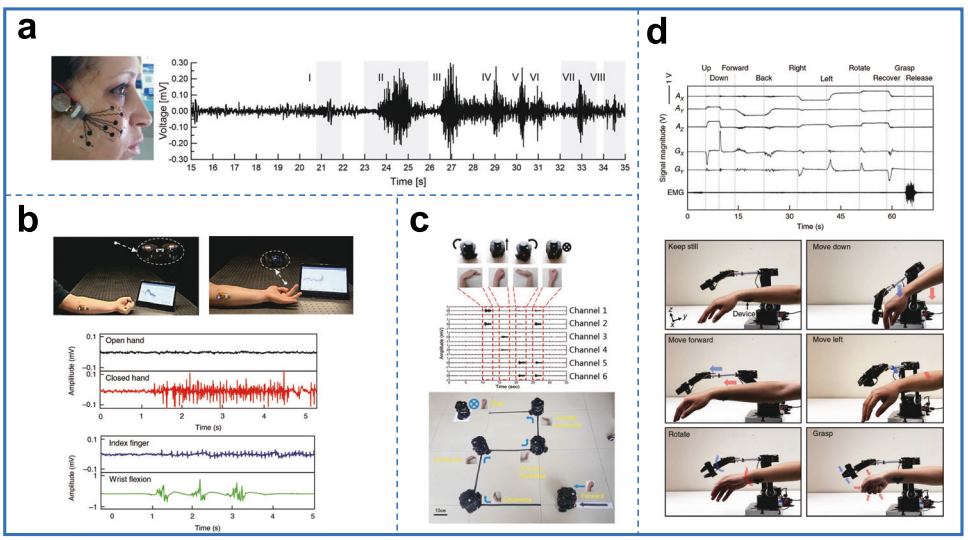

Fig. 18 The electrode arrays play a role in HMI. a The real-time recording of facial sEMG under a work environment. **b** The demonstration of flexible electronic systems for wireless HMI. **c** The gestures and the corresponding motion of the wheeled robot. **d** The photograph showing wireless robotic arm control and sEMG data from the sensing system. **a** Reproduced with permission[237]. Copyright @ 2018, Springer Nature. **b** Reproduced with permission[144]. Copyright @ 2020, Springer Nature. **c** Reproduced with permission[123]. Copyright @ 2019, American Chemical Society. **d** Reproduced with permission[27]. Copyright @ 2018, Springer Nature.

applications. The sEMG signals were recorded by using the fabricated electronic systems when different human hand gestures were made (Fig. 18c). Therefore, the meaning of gestures can be interpreted by analyzing the sEMG data. Notably, the wheeled robot can be precisely remote controlled by some gestures (such as wrist flexion, ulnar flexion, and wrist extension), which indicates that the hand gestures can be recognized.

In addition to the applications mentioned above, 3D structures can be adopted to design a noninvasive multifunctional HMI for promoting the functionality of sensing systems. Huang et al.[27] prepared 3D-integrated stretchable systems by using a layer-by-layer printing method. Notably, the acceleration, angular velocity, and sEMG signals can be measured by integration with different sensors. Subsequently, with real-time wireless data acquisition and

analysis, the mechanical arm can be wirelessly controlled by the sensing system for identification and imitation of the gestures of the human arm (Fig. 18d).

SUMMARY AND FUTURE PROSPECTS

The collection of sEMG signals is crucial for human healthcare and HMI applications. In this review, we have summarized the development of on-skin electrodes. Particularly, electrode materials including metal materials, carbon-based materials, and conductive polymers are introduced. Afterward, the properties of FNEs are discussed, such as adhesion, breathability, flexibility, and biocompatibility, which are essential for the performance and comfort of the flexible device. Subsequently, passive and active electrodes are introduced and then the amplifying sEMG signal role of active electrodes is emphasized. During the discussion of the active electrode array, we summarize its characteristics in terms of different TFT devices and amplifier designs. Compared with the passive electrodes array, the collection of sEMG signal by using active electrodes can reduce the influence of external noise and extremely amplify the SNR. Therefore, the advance of active electrode fabrication will not only promote the development of human healthcare but also support the HMI research for making the practical application possible. Despite the achievements of electrodes for sEMG signal recording, some challenges remain.

At present, skin electronic devices are prepared in a small area (several square centimeters), which cannot effectively locate the disease source and accurately decode the intentions of humans. It is urgent to break through the bottleneck of large-area skin electronic manufacturing. The large-scale physiological information collection of the human body is required for various applications. The large-area flexible electrode is enabled to capture high-quality bioelectrical signal recordings from human skin. Thus, extending the sizes of skin enable covering a larger scale of the human body. To fabricate large-area electrode arrays, traditional manufacturing techniques such as photolithography, etching processes, and high-vacuum deposition can be utilized, as well as cost-effective printing techniques such as inkjet printing and screen printing. The study of epidermal electrons has only made preliminary progress. The large-area skin electronic is easy to wear, however, limits the physiological function of the skin to sweat and heat dissipation. Therefore, large-area epidermal electrons require the substrate material to be breathable or even remove the substrate material. To achieve the breathability of FNEs, preparing nanomesh materials and designing porous substrates have been verified as two effective strategies at present. In addition, there is a trend for the integration of multiple sensors applied to flexible electronic skin. However, existing integrated systems face several challenges integration of various sensors, such as cross-sensitivity of different sensors, and hard-to-identify stimulus types and intensity because each sensor can respond to multiple stimuli. It is necessary to validate the system for adoption. Meanwhile, it is required that a large number of clinical studies are required to establish. Importantly, only when joint efforts have been made will the challenges of integration be achieved. Currently, the issue of cross-sensitivity arising from the integration of different sensors can be addressed through the manufacturing of sensors with lower cross-sensitivity, optimizing circuit design, performing signal processing on the outputs of different sensors, and so on.

In the process of weak sEMG signal acquisition, the SNR is an important standard to constantly measure signal quality. Reducing the influence of noise on sEMG is conducive to improving the SNR. The flexible EMG electrode made of highly adhesive materials has more contact with the skin. Therefore, the motion artifact generated by the relative motion between the electrode and the skin is reduced, which can improve the acquired table quality of the facial EMG signal. Therefore, combining material modification with structure design synergistically helps improve the adhesion of the electrode to the human skin.

In conclusion, despite challenges, flexible electrodes will advance and find broader applications by achieving the mentioned performance. The future of skin-electrode systems will emphasize wireless power, communication, and seamless skin-to-skin integration. Future flexible electrodes are hoped to be intelligent for acquiring bioelectrical signals in daily life. We predict that a critical trend in future development will be the integration of multifunctional systems into wearable devices to realize wireless and routine operations.

Received: 18 February 2023; Accepted: 5 August 2023;
Published online: 16 August 2023

REFERENCES

1. Zhou, Z., Zhang, H. S., Liu, J. Q. & Huang, W. Flexible electronics from intrinsically soft materials. *Giant* **6**, 100051 (2021).
2. Jang, K. I. et al. Self-assembled three dimensional network designs for soft electronics. *Nat. Commun.* **8**, 15894 (2017).
3. Imani, S. et al. A wearable chemical-electrophysiological hybrid biosensing system for real-time health and fitness monitoring. *Nat. Commun.* **7**, 11650 (2016).
4. Xu, S. et al. Soft microfluidic assemblies of sensors, circuits, and radios for the skin. *Science* **344**, 70–74 (2014).
5. Zhang, R. R., Lubin, J. A. & Kuo, J. S. Bioresorbable silicon electronic sensors for the brain. *Neurosurgery* **79**, N19 (2016).
6. Shin, S., Kang, M., Jung, J. & Kim, Y. T. Development of miniaturized wearable wristband type surface EMG measurement system for biometric authentication. *Electronics* **10**, 923 (2021).
7. Lim, S. et al. Transparent and stretchable interactive Human machine interface based on patterned graphene heterostructures. *Adv. Funct. Mater.* **25**, 375–383 (2015).
8. Kim, J. et al. Stretchable silicon nanoribbon electronics for skin prosthesis. *Nat. Commun.* **5**, 5747 (2014).
9. Yang, G. G. et al. Adhesive and hydrophobic bilayer hydrogel enabled on-skin biosensors for high-fidelity classification of human emotion. *Adv. Funct. Mater.* **32**, 2200457 (2022).
10. Kim, T., Park, J., Sohn, J., Cho, D. & Jeon, S. Bioinspired, highly stretchable, and conductive dry adhesives based on 1D-2D Hybrid carbon nanocomposites for all-in-one ECG electrodes. *ACS Nano* **10**, 4770–4778 (2016).
11. Lee, Y. et al. Self-adherent biodegradable gelatin-based hydrogel electrodes for electrocardiography monitoring. *Sensors* **20**, 5737 (2020).
12. Oh, H. et al. High density integration of stretchable inorganic thin film transistors with excellent performance and reliability. *Nat. Commun.* **13**, 4963 (2022).
13. Wang, Y. H. et al. Low-cost, μm-thick, tape-free electronic tattoo sensors with minimized motion and sweat artifacts. *NPJ Flex. Electron.* **2**, 6 (2018).
14. Ha, T. et al. A chest-laminated ultrathin and stretchable e-tattoo for the measurement of electrocardiogram, seismocardiogram, and cardiac time intervals. *Adv. Sci.* **6**, 1900290 (2019).
15. Wang, J. et al. Flexible electrodes for brain-computer interface system. *Adv. Mater.* e2211012 https://doi.org/10.1002/adma.202211012 (2022).
16. Hong, Y. J., Jeong, H., Cho, K. W., Lu, N. & Kim, D.-H. Wearable and implantable devices for cardiovascular healthcare: from monitoring to therapy based on flexible and stretchable electronics. *Adv. Funct. Mater.* **29**, 1808247 (2019).
17. Ren, L. et al. Flexible microneedle array electrode using magnetorheological drawing lithography for bio-signal monitoring. *Sens. Actuator A Phys.* **268**, 38–45 (2017).
18. Wolterink, G. et al. Development of soft sEMG sensing structures using 3D-printing technologies dagger. *Sensors* **20**, 4292 (2020).
19. Lapatki, B. G., van Dijk, J. P., Jonas, I. E., Zwarts, M. J. & Stegeman, D. F. A thin, flexible multielectrode grid for high-density surface EMG. *J. Appl. Physiol.* **96**, 327–336 (2004).
20. Simao, M., Mendes, N., Gibaru, O. & Neto, P. A review on electromyography decoding and pattern recognition for human-machine interaction. *IEEE Access* **7**, 39564–39582 (2019).
21. Zhang, L. et al. Wearable circuits sintered at room temperature directly on the skin surface for health monitoring. *ACS Appl. Mater. Interfaces* **12**, 45504–45515 (2020).

22. Kim, D. H. et al. Epidermal electronics. *Science* **333**, 838–843 (2011).
23. Jeong, J. W. et al. Materials and optimized designs for human-machine interfaces via epidermal electronics. *Adv. Mater.* **25**, 6839–6846 (2013).
24. Jang, K. I. et al. Rugged and breathable forms of stretchable electronics with adherent composite substrates for transcutaneous monitoring. *Nat. Commun.* **5**, 4779 (2014).
25. Matsuhisa, N. et al. Printable elastic conductors with a high conductivity for electronic textile applications. *Nat. Commun.* **6**, 7461 (2015).
26. Han, S. et al. Mechanically reinforced skin-electronics with networked nanocomposite elastomer. *Adv. Mater.* **28**, 10257–10265 (2016).
27. Huang, Z. et al. Three-dimensional integrated stretchable electronics. *Nat. Electron.* **1**, 473–480 (2018).
28. Tian, L. et al. Large-area MRI-compatible epidermal electronic interfaces for prosthetic control and cognitive monitoring. *Nat. Biomed. Eng.* **3**, 194–205 (2019).
29. Zhang, L. et al. Fully organic compliant dry electrodes self-adhesive to skin for long-term motion-robust epidermal biopotential monitoring. *Nat. Commun.* **11**, 13 (2020).
30. Wang, W. et al. Strain-insensitive intrinsically stretchable transistors and circuits. *Nat. Electron.* **4**, 143–150 (2021).
31. Jiang, Y. W. et al. Topological supramolecular network enabled high-conductivity, stretchable organic bioelectronics. *Science* **375**, 1411–1417 (2022).
32. Lee, W. & Someya, T. Emerging trends in flexible active multielectrode arrays. *Chem. Mater.* **31**, 6347–6358 (2019).
33. Amjadi, M., Kyung, K.-U., Park, I. & Sitti, M. Stretchable, skin-mountable, and wearable strain sensors and their potential applications: a review. *Adv. Funct. Mater.* **26**, 1678–1698 (2016).
34. Khan, Y., Ostfeld, A. E., Lochner, C. M., Pierre, A. & Arias, A. C. Monitoring of vital signs with flexible and wearable medical devices. *Adv. Mater.* **28**, 4373–4395 (2016).
35. Ma, Z. et al. Advanced electronic skin devices for healthcare applications. *J. Mater. Chem. B* **7**, 173–197 (2019).
36. Araki, T. et al. Long-term implantable, flexible, and transparent neural interface based on Ag/Au core-shell nanowires. *Adv. Healthc. Mater.* **8**, 1900130 (2019).
37. Waasdorp, R. et al. Combining ultrafast ultrasound and high-density EMG to assess local electromechanical muscle dynamics: a feasibility study. *IEEE Access* **9**, 45277–45288 (2021).
38. Chortos, A. & Bao, Z. Skin-inspired electronic devices. *Mater. Today* **17**, 321–331 (2014).
39. Rojas, W. A. G., Beck, M. E., Sangwan, V. K., Guo, S. L. & Hersam, M. C. Ohmic-contact-gated carbon nanotube transistors for high-performance analog amplifiers. *Adv. Mater.* **33**, 2100994 (2021).
40. Lee, W. et al. Transparent, conformable, active multielectrode array using organic electrochemical transistors. *Proc. Natl. Acad. Sci. USA* **114**, 10554–10559 (2017).
41. Sekitani, T. et al. Ultraflexible organic amplifier with biocompatible gel electrodes. *Nat. Commun.* **7**, 11425 (2016).
42. Braendlein, M., Lonjaret, T., Leleux, P., Badier, J. M. & Malliaras, G. G. Voltage amplifier based on organic electrochemical transistor. *Adv. Sci.* **4**, 1600247 (2017).
43. Kizilkan, E. & Gorb, S. N. Bioinspired further enhanced dry adhesive by the combined effect of the microstructure and surface free-energy increase. *ACS Appl. Mater. Interfaces* **10**, 26752–26758 (2018).
44. Liu, Z. Y. et al. High-adhesion stretchable electrodes based on nanopile interlocking. *Adv. Mater.* **29**, 1603382 (2017).
45. Kim, J. et al. Epidermal electronics with advanced capabilities in near-field communication. *Small* **11**, 906–912 (2015).
46. Lee, S. M. et al. Self-adhesive epidermal carbon nanotube electronics for tether-free long-term continuous recording of biosignals. *Sci. Rep.* **4**, 6074 (2014).
47. Huang, X. et al. Stretchable, wireless sensors and functional substrates for epidermal characterization of sweat. *Small* **10**, 3083–3090 (2014).
48. Yeo, W.-H. et al. Multifunctional epidermal electronics printed directly onto the skin. *Adv. Mater.* **25**, 2773–2778 (2013).
49. Yang, S. Y. et al. A bio-inspired swellable microneedle adhesive for mechanical interlocking with tissue. *Nat. Commun.* **4**, 1702 (2013).
50. Kwak, M. K., Jeong, H. E. & Suh, K. Y. Rational design and enhanced biocompatibility of a dry adhesive medical skin patch. *Adv. Mater.* **23**, 3949–3953 (2011).
51. Reeder, J. T. et al. Waterproof, electronics-enabled, epidermal microfluidic devices for sweat collection, biomarker analysis, and thermography in aquatic settings. *Sci. Adv.* **5**, eaau6356 (2019).
52. Kwon, Y. T. et al. Breathable, large-area epidermal electronic systems for recording electromyographic activity during operant conditioning of H-reflex. *Biosens. Bioelectron.* **165**, 112404 (2020).
53. Xu, R. D. et al. Breathable Kirigami-shaped ionotronic e-textile with touch/strain sensing for friendly epidermal electronics. *Adv. Fiber Mater.* **4**, 1525–1534 (2022).
54. Yang, Y. et al. Breathable electronic skins for daily physiological signal monitoring. *Nanomicro Lett.* **14**, 161 (2022).
55. Lo, L. W. et al. Stretchable sponge electrodes for long-term and motion-artifact-tolerant recording of high-quality electrophysiologic signals. *ACS Nano* **16**, 11792–11801 (2022).
56. Min, H. et al. Highly air/water-permeable hierarchical mesh architectures for stretchable underwater electronic skin patches. *ACS Appl. Mater. Interfaces* **12**, 14425–14432 (2020).
57. Miyamoto, A. et al. Inflammation-free, gas-permeable, lightweight, stretchable on-skin electronics with nanomeshes. *Nat. Nanotechnol.* **12**, 907–913 (2017).
58. Ji, Y. et al. Flexible metal electrodes by femtosecond laser-activated deposition for human-machine interfaces. *ACS Appl. Mater. Interfaces* **14**, 11971–11980 (2022).
59. Choi, S. et al. Highly conductive, stretchable and biocompatible Ag-Au core-sheath nanowire composite for wearable and implantable bioelectronics. *Nat. Nanotechnol.* **13**, 1048–1056 (2018).
60. Alam, A. et al. Flexible heterogeneously integrated low form factor wireless multi-channel surface electromyography (sEMG) device. in *IEEE Electronic Components and Technology Conference*, 1544–1549 (IEEE, 2021) .
61. Yang, H. et al. Adhesive biocomposite electrodes on sweaty skin for long-term continuous electrophysiological monitoring. *ACS Mater. Lett.* **2**, 478–484 (2020).
62. Ye, G. et al. A Lamellibranchia-inspired epidermal electrode for electrophysiology. *Mater. Horiz.* **8**, 1047–1057 (2021).
63. Yamamoto, Y. et al. Efficient skin temperature sensor and stable gel-less sticky ECG sensor for a wearable flexible healthcare patch. *Adv. Healthc. Mater.* **6**, 1700495 (2017).
64. Kim, J. et al. An elastomer for epidermal electronics with adjustable adhesion force and stretchability obtained via a reverse-micelle-induced process. *J. Mater. Chem. C.* **6**, 2210–2215 (2018).
65. Jeong, S. H., Zhang, S., Hjort, K., Hilborn, J. & Wu, Z. G. PDMS-based elastomer tuned soft, stretchable, and sticky for epidermal electronics. *Adv. Mater.* **28**, 5830 (2016).
66. Lee, B. K. et al. Silicone-based adhesives with highly tunable adhesion force for skin-contact applications. *Adv. Healthc. Mater.* **6**, 1700621 (2017).
67. Sun, S. M., Li, M. L. & Liu, A. A review on mechanical properties of pressure sensitive adhesives. *Int. J. Adhes. Adhes.* **41**, 98–106 (2013).
68. Wu, J. et al. Unidirectional water-penetration composite fibrous film via electrospinning. *Soft Matter* **8**, 5996–5999 (2012).
69. Zhao, Y., Wang, H. X., Zhou, H. & Lin, T. Directional fluid transport in thin porous materials and its functional applications. *Small* **13**, 1601070 (2017).
70. Fan, Y. J. et al. Highly robust, transparent, and breathable epidermal electrode. *ACS Nano* **12**, 9326–9332 (2018).
71. Sun, B. H. et al. Gas-permeable, multifunctional on-skin electronics based on laser-induced porous graphene and sugar-templated elastomer sponges. *Adv. Mater.* **30**, 1804327 (2018).
72. Heikenfeld, J. et al. Wearable sensors: modalities, challenges, and prospects. *Lab Chip* **18**, 217–248 (2018).
73. Zhou, W. X. et al. Gas-permeable, ultrathin, stretchable epidermal electronics with porous electrodes. *ACS Nano* **14**, 5798–5805 (2020).
74. Won, S. M. et al. Recent advances in materials, devices, and systems for neural interfaces. *Adv. Mater.* **30**, 1800534 (2018).
75. Minev, I. R. et al. Electronic dura mater for long-term multimodal neural interfaces. *Science* **347**, 159–163 (2015).
76. Yang, X. Q. et al. All-nanofiber-based Janus epidermal electrode with directional sweat permeability for artifact-free biopotential monitoring. *Small* **18**, 2106477 (2022).
77. Zheng, Y. et al. Ultrathin and highly breathable electronic tattoo for sensing multiple signals imperceptibly on the skin. *Nano Energy* **107**, 108092 (2023).
78. Takei, K. et al. Nanowire active-matrix circuitry for low-voltage macroscale artificial skin. *Nat. Mater.* **9**, 821–826 (2010).
79. Jung, J. M. et al. Development of PDMS-based flexible dry type sEMG electrodes by micromachining technologies. *Appl. Phys. A* **116**, 1395–1401 (2014).
80. Chen, X. Making electrodes stretchable. *Small Methods* **1**, 1600029 (2017).
81. Cheng, J. H. et al. Wet-adhesive elastomer for liquid metal-based conformal epidermal electronics. *Adv. Funct. Mater.* **32**, 2200444 (2022).
82. Blau, R. et al. Intrinsically stretchable block copolymer based on PEDOT:PSS for improved performance in bioelectronic applications. *ACS Appl. Mater. Interfaces* **14**, 4823–4835 (2022).
83. Pan, S. et al. Mechanically interlocked hydrogel–elastomer hybrids for on-skin electronics. *Adv. Funct. Mater.* **30**, 1909540 (2020).
84. Cheng, Y. et al. An elastic and damage-tolerant dry epidermal patch with robust skin adhesion for bioelectronic interfacing. *ACS Nano* **16**, 18608–18620 (2022).
85. Yang, Y. R. et al. A laser-engraved wearable sensor for sensitive detection of uric acid and tyrosine in sweat. *Nat. Biotechnol.* **38**, 217–224 (2020).

86. Xu, K. C. et al. Highly stable kirigami-structured stretchable strain sensors for perdurable wearable electronics. *J. Mater. Chem. C.* **7**, 9609–9617 (2019).
87. Shi, X. et al. Large-area display textiles integrated with functional systems. *Nature* **591**, 240–245 (2021).
88. Kaltenbrunner, M. et al. An ultra-lightweight design for imperceptible plastic electronics. *Nature* **499**, 458–463 (2013).
89. Chen, G. et al. Plasticizing silk protein for on-skin stretchable electrodes. *Adv. Mater.* **30**, 1800129 (2018).
90. Wang, C., Yokota, T. & Someya, T. Natural biopolymer-based biocompatible conductors for stretchable bioelectronics. *Chem. Rev.* **121**, 2109–2146 (2021).
91. Kim, J. Y. et al. Leaf-inspired homeostatic cellulose biosensors. *Sci. Adv.* **7**, eabe7432 (2021).
92. Zhang, Y. J. & Tao, T. H. Skin-friendly electronics for acquiring human physiological signatures. *Adv. Mater.* **31**, 1905767 (2019).
93. Cai, P. Q. et al. Locally coupled electromechanical interfaces based on cytoadhesion-inspired hybrids to identify muscular excitation-contraction signatures. *Nat. Commun.* **11**, 2183 (2020).
94. Ma, Y. et al. Soft elastomers with ionic liquid-filled cavities as strain isolating substrates for wearable electronics. *Small* **13**, 1602954 (2017).
95. Gandla, S. et al. Ultrafast prototyping of large-area stretchable electronic systems by laser ablation technique for controllable robotic arm operations. *IEEE Trans. Ind. Electron.* **69**, 4245–4253 (2022).
96. Hou, K. X. et al. A puncture-resistant and self-healing conductive gel for multifunctional electronic skin. *Adv. Funct. Mater.* **31**, 2107006 (2021).
97. Zhou, X. et al. Self-healing, stretchable, and highly adhesive hydrogels for epidermal patch electrodes. *Acta Biomater.* **139**, 296–306 (2022).
98. Song, J. et al. Stretchable and self-healable graphene-polymer conductive composite for wearable EMG sensor. *Polymers* **14**, 3766 (2022).
99. Kim, S. H. et al. Mechanically and electrically durable, stretchable electronic textiles for robust wearable electronics. *RSC Adv.* **11**, 22327–22333 (2021).
100. Lee, Y. et al. Soft electronics enabled ergonomic human-computer interaction for swallowing training. *Sci. Rep.* **7**, 46697 (2017).
101. Koo, J. H. et al. Wearable electrocardiogram monitor using carbon nanotube electronics and color-tunable organic light-emitting diodes. *ACS Nano* **11**, 10032–10041 (2017).
102. Lu, S. & Franklin, A. D. Printed carbon nanotube thin-film transistors: progress on printable materials and the path to applications. *Nanoscale* **12**, 23371–23390 (2020).
103. Liang, G. et al. A PDMS-based integrated stretchable microelectrode array (isMEA) for neural and muscular surface interfacing. *IEEE Trans. Biomed. Circuits Syst.* **7**, 1–10 (2013).
104. Xu, B. X. et al. An epidermal stimulation and sensing platform for sensorimotor prosthetic control, management of lower back exertion, and electrical muscle activation. *Adv. Mater.* **28**, 4462–4471 (2016).
105. Laferriere, P., Lemaire, E. D. & Chan, A. D. C. Surface electromyographic signals using dry electrodes. *IEEE Trans. Instrum. Meas.* **60**, 3259–3268 (2011).
106. Zou, W. H. et al. Electrohydrodynamic direct-writing fabrication of microstructure-enhanced microelectrode arrays for customized and curved physiological electronics. *Adv. Mater. Interfaces* **9**, 2201197 (2022).
107. Kim, N., Lim, T., Song, K., Yang, S. & Lee, J. Stretchable multichannel electromyography sensor array covering large area for controlling home electronics with distinguishable signals from multiple muscles. *ACS Appl. Mater. Interfaces* **8**, 21070–21076 (2016).
108. He, K. et al. An on-skin electrode with anti-epidermal-surface-lipid function based on a zwitterionic polymer brush. *Adv. Mater.* **32**, 2001130 (2020).
109. Wang, B., Maslik, J., Hellman, O., Gumiero, A. & Hjort, K. Supercooled liquid Ga stretchable electronics. *Adv. Funct. Mater.* **33**, 2300036 (2023).
110. Choi, H. et al. Highly stretchable and strain-insensitive liquid metal based elastic kirigami electrodes (LM-eKE). *Adv. Funct. Mater.* **33**, 2301388 (2023).
111. Ma, X. H. et al. Highly permeable and ultrastretchable liquid metal micromesh for skin-attachable electronics. *ACS Mater. Lett.* **4**, 634–641 (2022).
112. Li, X. et al. A self-supporting, conductor-exposing, stretchable, ultrathin, and recyclable kirigami-structured liquid metal paper for multifunctional E-skin. *ACS Nano* **16**, 5909–5919 (2022).
113. Lim, T. et al. Multiscale material engineering of a conductive polymer and a liquid metal platform for stretchable and biostable human-machine-interface bioelectronic applications. *ACS Mater. Lett.* **4**, 2289–2297 (2022).
114. Kim, Y., Song, J., An, S., Shin, M. & Son, D. Soft liquid metal-based conducting composite with robust electrical durability for a wearable electrocardiogram sensor. *Polymers* **14**, 3409 (2022).
115. Yoon, S. et al. Highly stretchable metal-polymer hybrid conductors for wearable and self-cleaning sensors. *NPG Asia Mater.* **13**, 4 (2021).
116. Yun, I. et al. Stable bioelectric signal acquisition using an enlarged surface-area flexible skin electrode. *ACS Appl. Electron. Mater.* **3**, 1842–1851 (2021).
117. M, S. R. et al. Dry electrodes for surface electromyography based on architectured titanium thin films. *Materials* **13**, 2135 (2020).
118. Myers, A. C., Huang, H. & Zhu, Y. Wearable silver nanowire dry electrodes for electrophysiological sensing. *RSC Adv.* **5**, 11627–11632 (2015).
119. Xu, Y. et al. Multiscale porous elastomer substrates for multifunctional on-skin electronics with passive-cooling capabilities. *Proc. Natl. Acad. Sci. USA* **117**, 205–213 (2020).
120. Pan, S. W. et al. Mechanically interlocked hydrogel-elastomer hybrids for on-skin electronics. *Adv. Funct. Mater.* **30**, 9 (2020).
121. Zhu, K., Guo, W., Yang, G., Li, Z. & Wu, H. High-fidelity recording of EMG signals by multichannel on-skin electrode arrays from target muscles for effective human–machine interfaces. *ACS Appl. Electron. Mater.* **3**, 1350–1358 (2021).
122. Zhou, Y. et al. Multichannel noninvasive human–machine interface via stretchable μm thick sEMG patches for robot manipulation. *J. Micromech. Microeng.* **28**, 014005 (2018).
123. Guo, W. et al. Matrix-independent highly conductive composites for electrodes and interconnects in stretchable electronics. *ACS Appl. Mater. Interfaces* **11**, 8567–8575 (2019).
124. Qiao, Y. C. et al. Electromyogram-strain synergetic intelligent artificial throat. *Chem. Eng. J.* **449**, 137741 (2022).
125. Yan, X. L. et al. Highly breathable, surface-hydrophobic and wet-adhesive silk based epidermal electrode for long-term electrophysiological monitoring. *Compos Sci. Technol.* **230**, 109751 (2022).
126. Yang, X. Q. et al. Ultrathin, stretchable, and breathable epidermal electronics based on a facile bubble blowing method. *Adv. Electron. Mater.* **6**, 2000306 (2020).
127. Chae, H. et al. Laser-processed nature-inspired deformable structures for breathable and reusable electrophysiological sensors toward controllable home electronic appliances and psychophysiological stress monitoring. *ACS Appl. Mater. Interfaces* **11**, 28387–28396 (2019).
128. Kim, D. et al. Biocompatible cost-effective electrophysiological monitoring with oxidation-free Cu-Au core-shell nanowire. *Adv. Mater. Technol.* **5**, 2000661 (2020).
129. Yao, S. S. et al. Ultrasoft porous 3D conductive dry electrodes for electrophysiological sensing and myoelectric control. *Adv. Mater. Technol.* **7**, 2101637 (2022).
130. Nawrocki, R. A. et al. Self-adhesive and ultra-conformable, sub-300 nm dry thin-film electrodes for surface monitoring of biopotentials. *Adv. Funct. Mater.* **28**, 1803279 (2018).
131. Reis Carneiro, M., Majidi, C. & Tavakoli, M. Multi-electrode printed bioelectronic patches for long-term electrophysiological monitoring. *Adv. Funct. Mater.* **32**, 2205956 (2022).
132. Liang, X. et al. Carbon-based SERS biosensor: from substrate design to sensing and bioapplication. *NPG Asia Mater.* **13**, 8 (2021).
133. Liang, X. P. et al. Stable and biocompatible carbon nanotube ink mediated by silk protein for printed electronics. *Adv. Mater.* **32**, 2000165 (2020).
134. Li, B. M. et al. Iron-on carbon nanotube (CNT) thin films for biosensing e-textile applications. *Carbon* **168**, 673–683 (2020).
135. Kabiri Ameri, S. et al. Graphene electronic tattoo sensors. *ACS Nano* **11**, 7634–7641 (2017).
136. Xia, H. Q. et al. Mediator-free electron-transfer on patternable hierarchical meso/macro porous bienzyme interface for highly-sensitive sweat glucose and surface electromyography monitoring. *Sens. Actuators B Chem.* **312**, 127962 (2020).
137. Kang, B. C. & Ha, T. J. Wearable carbon nanotube based dry-electrodes for electrophysiological sensors. *Jpn. J. Appl Phys.* **57**, 05GD02 (2018).
138. Xu, X. et al. Wearable CNT/$Ti_3C_2T_x$ MXene/PDMS composite strain sensor with enhanced stability for real-time human healthcare monitoring. *Nano Res.* **14**, 2875–2883 (2021).
139. Gogurla, N., Kim, Y., Cho, S., Kim, J. & Kim, S. Multifunctional and ultrathin electronic tattoo for on-skin diagnostic and therapeutic applications. *Adv. Mater.* **33**, 2008308 (2021).
140. Nag, A. et al. Graphene-based wearable temperature sensors: a review. *Mater. Des.* **221**, 110971 (2022).
141. Novoselov, K. S. et al. Electric field effect in atomically thin carbon films. *Science* **306**, 666–669 (2004).
142. Wang, F., Liu, L. & Li, W. J. Graphene-based glucose sensors: a brief review. *IEEE Trans. Nanobiosci.* **14**, 818–834 (2015).
143. Xu, T., Zhang, Z. & Qu, L. Graphene-based fibers: recent advances in preparation and application. *Adv. Mater.* **32**, 1901979 (2020).
144. Kwon, Y. T. et al. All-printed nanomembrane wireless bioelectronics using a biocompatible solderable graphene for multimodal human-machine interfaces. *Nat. Commun.* **11**, 3450 (2020).
145. Li, Z. et al. On-skin graphene electrodes for large area electrophysiological monitoring and human-machine interfaces. *Carbon* **164**, 164–170 (2020).
146. Yun, Y. J. et al. Highly elastic graphene-based electronics toward electronic skin. *Adv. Funct. Mater.* **27**, 1701513 (2017).
147. Yang, J. et al. Facile fabrication of robust and reusable PDMS supported graphene dry electrodes for wearable electrocardiogram monitoring. *Adv. Mater. Technol.* **6**, 2100262 (2021).

148. Yapici, M. K., Alkhidir, T., Samad, Y. A. & Liao, K. Graphene-clad textile electrodes for electrocardiogram monitoring. *Sens. Actuators B Chem.* **221**, 1469–1474 (2015).
149. Dong, J. C. et al. Ultra-stretchable and superhydrophobic textile-based bioelectrodes for robust self-cleaning and personal health monitoring. *Nano Energy* **97**, 107160 (2022).
150. Tian, H. et al. Bioinspired dual-channel speech recognition using graphene-based electromyographic and mechanical sensors. *Cell Rep. Phys. Sci.* **3**, 101075 (2022).
151. Liang, X. P. et al. Hydrophilic, breathable, and washable graphene decorated textile assisted by silk sericin for integrated multimodal smart wearables. *Adv. Funct. Mater.* **32**, 2200162 (2022).
152. Pan, X. et al. A bionic tactile plastic hydrogel-based electronic skin constructed by a nerve-like nanonetwork combining stretchable, compliant, and self-healing properties. *Chem. Eng. J.* **379**, 1909540 (2020).
153. Bihar, E. et al. Fully printed all-polymer tattoo/textile electronics for electromyography. *Flex. Print. Electron.* **3**, 034004 (2018).
154. Leleux, P. et al. Conducting polymer electrodes for electroencephalography. *Adv. Healthc. Mater.* **3**, 490–493 (2014).
155. Sessolo, M. et al. Easy-to-fabricate conducting polymer microelectrode arrays. *Adv. Mater.* **25**, 2135–2139 (2013).
156. He, H. et al. Biocompatible conductive polymers with high conductivity and high stretchability. *ACS Appl. Mater. Interfaces* **11**, 26185–26193 (2019).
157. Zucca, A. et al. Tattoo conductive polymer nanosheets for skin-contact applications. *Adv. Healthc. Mater.* **4**, 983–990 (2015).
158. Velasco-Bosom, S. et al. Conducting polymer-ionic liquid electrode arrays for high-density surface electromyography. *Adv. Healthc. Mater.* **10**, 2100374 (2021).
159. Ferrari, L. M. et al. Ultraconformable temporary tattoo electrodes for electrophysiology. *Adv. Sci.* **5**, 1700771 (2018).
160. Zhao, Y. et al. Ultra-conformal skin electrodes with synergistically enhanced conductivity for long-time and low-motion artifact epidermal electrophysiology. *Nat. Commun.* **12**, 4880 (2021).
161. Tang, W. J. et al. Delamination-resistant imperceptible bioelectrode for robust electrophysiological signals monitoring. *ACS Mater. Lett.* **3**, 1385–1393 (2021).
162. Meng, L., Fu, Q. J., Hao, S. W., Xu, F. & Yang, J. Self-adhesive, biodegradable silk-based dry electrodes for epidermal electrophysiological monitoring. *Chem. Eng. J.* **427**, 131999 (2022).
163. Tan, P. et al. Solution-processable, soft, self-adhesive, and conductive polymer composites for soft electronics. *Nat. Commun.* **13**, 358 (2022).
164. Zheng, S. J. et al. Moisture-wicking, breathable, and intrinsically antibacterial electronic skin based on dual-gradient poly(ionic liquid) nanofiber membranes. *Adv. Mater.* **34**, 2106570 (2022).
165. Roberts, T. et al. Flexible inkjet-printed multielectrode arrays for neuromuscular cartography. *Adv. Healthc. Mater.* **5**, 1462–1470 (2016).
166. Luo, J. B. et al. A bio-adhesive ion-conducting organohydrogel as a high-performance non-invasive interface for bioelectronics. *Chem. Eng. J.* **427**, 130886 (2022).
167. Ouyang, J. Y. et al. Stretchable and self-adhesive PEDOT:PSS blend with high sweat tolerance as conformal biopotential dry electrodes. *ACS Appl. Mater. Interfaces* **14**, 39159–39171 (2022).
168. Fang, Y. et al. Solution-processed submicron free-standing, conformal, transparent, breathable epidermal electrodes. *ACS Appl. Mater. Interfaces* **12**, 23689–23696 (2020).
169. Malesevic, N. et al. A database of multi-channel intramuscular electromyogram signals during isometric hand muscles contractions. *Sci. Data* **7**, 10 (2020).
170. Hua, Q. et al. Skin-inspired highly stretchable and conformable matrix networks for multifunctional sensing. *Nat. Commun.* **9**, 244 (2018).
171. Wang, Y. H. et al. Electrically compensated, tattoo-like electrodes for epidermal electrophysiology at scale. *Sci. Adv.* **6**, eabd0996 (2020).
172. Fan, J. A. et al. Fractal design concepts for stretchable electronics. *Nat. Commun.* **5**, 3266 (2014).
173. Scalisi, R. G. et al. Inkjet printed flexible electrodes for surface electromyography. *Org. Electron.* **18**, 89–94 (2015).
174. Poppendieck, W. et al. Development of multi-channel intramuscular EMG recording electrodes. *Biomed Tech.* **58**, Sl-1-Track-O (2013).
175. Bihar, E. et al. Inkjet-printed PEDOT:PSS electrodes on paper for electrocardiography. *Adv. Healthc. Mater.* **6**, 1601167 (2017).
176. Kim, K. et al. Low-voltage, high-sensitivity and high-reliability bimodal sensor array with fully inkjet-printed flexible conducting electrode for low power consumption electronic skin. *Nano Energy* **41**, 301–307 (2017).
177. Zhang, X., Tang, X., Wei, Z. Q., Chen, X. & Chen, X. Model-based sensitivity analysis of EMG clustering index with respect to motor unit properties: investigating post-stroke FDI muscle. *IEEE Trans. Neural Syst. Rehabil. Eng.* **28**, 1836–1845 (2020).
178. Cui, H. et al. EEG-based emotion recognition using an end-to-end regional-asymmetric convolutional neural network. *Knowl. Based Syst.* **205**, 106243 (2020).
179. Zhang, X. et al. Spatial filtering for enhanced high-density surface electromyographic examination of neuromuscular changes and its application to spinal cord injury. *J. Neuroeng. Rehabilitation.* **17**, 160 (2020).
180. Xiang, C., Li, Y., Hu, R., Zhang, X. & Chen, X. Hand gesture recognition based on surface electromyography using convolutional neural network with transfer learning method. *IEEE J. Biomed. Health Inf.* **25**, 1292–1304 (2021).
181. Li, Y., Xiang, C., Zhang, X., Wang, K. & Wang, Z. J. A sign-component-based framework for Chinese sign language recognition using accelerometer and sEMG data. *Ieee. Trans. Biomed. Eng.* **59**, 2695–2704 (2012).
182. Xu, Z. et al. A framework for hand gesture recognition based on accelerometer and EMG sensors. *IEEE Trans. Syst. Man Cybern. Syst.* **41**, 1064–1076 (2011).
183. Peng, H.-L. et al. Flexible dry electrode based on carbon nanotube/polymer hybrid micropillars for biopotential recording. *Sens. Actuator A Phys.* **235**, 48–56 (2015).
184. Dong, Z., Chen, X., Deng, H. & Zhang, Y. Design of differential concentric ring sEMG electrode array based on flexible printed circuit. *J. Electron. Meas. Instrum.* **26**, 359–366 (2013).
185. Xu, Y. et al. Oxide TFT frontend amplifiers for flexible sensing systems. *IEEE Trans. Electron Devices* **68**, 6190–6196 (2021).
186. Wang, N., Yang, A., Fu, Y., Li, Y. & Yan, F. Functionalized organic thin film transistors for biosensing. *Acc. Chem. Res.* **52**, 277–287 (2019).
187. Myny, K. The development of flexible integrated circuits based on thin-film transistors. *Nat. Electron.* **1**, 30–39 (2018).
188. Cantarella, G. et al. Review of recent trends in flexible metal oxide thin-film transistors for analog applications. *Flex. Print. Electron.* **5**, 033001 (2020).
189. Chen, H., Cao, Y., Zhang, J. & Zhou, C. Large-scale complementary macroelectronics using hybrid integration of carbon nanotubes and IGZO thin-film transistors. *Nat. Commun.* **5**, 4097 (2014).
190. Gao, Y. et al. High-performance flexible thin-film transistors based on single-crystal-like silicon epitaxially grown on metal tape by roll-to-roll continuous deposition process. *ACS Appl. Mater. Interfaces* **8**, 29565–29572 (2016).
191. Kim, B. H. et al. Three-dimensional silicon electronic systems fabricated by compressive buckling process. *ACS Nano* **12**, 4164–4171 (2018).
192. Asadirad, M. et al. High-performance flexible thin-film transistors based on single-crystal-like germanium on glass. *Adv. Electron. Mater.* **2**, 1600041 (2016).
193. Wang, S. et al. Skin electronics from scalable fabrication of an intrinsically stretchable transistor array. *Nature* **555**, 83–88 (2018).
194. Sugiyama, M. et al. An ultraflexible organic differential amplifier for recording electrocardiograms. *Nat. Electron.* **2**, 351–360 (2019).
195. Lee, W. et al. Integration of organic electrochemical and field-effect transistors for ultraflexible, high temporal resolution electrophysiology arrays. *Adv. Mater.* **28**, 9722–9728 (2017).
196. Fuketa, H. et al. 1 um-thickness ultra-flexible and high electrode-density surface electromyogram measurement sheet with 2 V organic transistors for prosthetic hand control. *IEEE Trans. Biomed. Circuits Syst.* **8**, 824–833 (2014).
197. Kondo, M. et al. Highly-ordered triptycene modifier layer based on blade coating for ultraflexible organic transistors. *Sci. Rep.* **9**, 9200 (2019).
198. Lee, M. Y., Lee, H. R., Park, C. H., Han, S. G. & Oh, J. H. Organic transistor-based chemical sensors for wearable bioelectronics. *Acc. Chem. Res.* **51**, 2829–2838 (2018).
199. Oh, J. Y. et al. Intrinsically stretchable and healable semiconducting polymer for organic transistors. *Nature* **539**, 411–415 (2016).
200. Walter, S. R. et al. In-situ probe of gate dielectric-semiconductor interfacial order in organic transistors: origin and control of large performance sensitivities. *J. Am. Chem. Soc.* **134**, 11726–11733 (2012).
201. LeComber, P. G., Spear, W. E. & Gaith, A. Amorphous-Silicon Field-Effect Device and Possible Application. *Electron. Lett.* **15**, 179–181 (1979).
202. Depp, S. W., Juliana, A. & Huth, B. G. Polysilicon FET devices for large area input/output applications. In *1980 International Electron Devices Meeting* (IEEE, 1980).
203. Chiang, C. H. et al. Development of a neural interface for high-definition, long-term recording in rodents and nonhuman primates. *Sci. Transl. Med.* **12**, eaay4682 (2020).
204. Fang, H. et al. Capacitively coupled arrays of multiplexed flexible silicon transistors for long-term cardiac electrophysiology. *Nat. Biomed. Eng.* **1**, 0038 (2017).
205. Han, M. et al. Catheter-integrated soft multilayer electronic arrays for multiplexed sensing and actuation during cardiac surgery. *Nat. Biomed. Eng.* **4**, 997–1009 (2020).
206. Song, E. et al. Flexible electronic/optoelectronic microsystems with scalable designs for chronic biointegration. *Proc. Natl. Acad. Sci. USA* **116**, 15398–15406 (2019).
207. Won, S. M., Song, E., Reeder, J. T. & Rogers, J. A. Emerging modalities and implantable technologies for neuromodulation. *Cell* **181**, 115–135 (2020).
208. Song, E., Li, J., Won, S. M., Bai, W. & Rogers, J. A. Materials for flexible bioelectronic systems as chronic neural interfaces. *Nat. Mater.* **19**, 590–603 (2020).
209. Song, E. et al. Miniaturized electromechanical devices for the characterization of the biomechanics of deep tissue. *Nat. Biomed. Eng.* **5**, 759–771 (2021).

210. Song, E. et al. Recent advances in microsystem approaches for mechanical characterization of soft biological tissues. *Microsyst. Nanoeng.* **8**, 77 (2022).
211. Minemawari, H. et al. Inkjet printing of single-crystal films. *Nature* **475**, 364–367 (2011).
212. Giri, G. et al. Tuning charge transport in solution-sheared organic semiconductors using lattice strain. *Nature* **480**, 504–508 (2011).
213. Nakayama, K. et al. Patternable solution-crystallized organic transistors with high charge carrier mobility. *Adv. Mater.* **23**, 1626–1629 (2011).
214. Smith, J. et al. Solution-processed small molecule-polymer blend organic thin-film transistors with hole mobility greater than 5 cm^2/Vs. *Adv. Mater.* **24**, 2441–2446 (2012).
215. Tsao, H. N. et al. Ultrahigh mobility in polymer field-effect transistors by design. *J. Am. Chem. Soc.* **133**, 2605–2612 (2011).
216. Zschieschang, U., Waizmann, U., Weis, J., Borchert, J. W. & Klauk, H. Nanoscale flexible organic thin-film transistors. *Sci. Adv.* **8**, eabm9845 (2022).
217. He, D. W. et al. Ultrahigh mobility and efficient charge injection in monolayer organic thin-film transistors on boron nitride. *Sci. Adv.* **3**, e1701186 (2017).
218. Yao, J. J. et al. Significant improvement of semiconducting performance of the diketopyrrolopyrrole-quaterthiophene conjugated polymer through side-chain engineering via hydrogen-bonding. *J. Am. Chem. Soc.* **138**, 173–185 (2016).
219. Xu, J. et al. Highly stretchable polymer semiconductor films through the nanoconfinement effect. *Science* **355**, 59–64 (2017).
220. Zhao, X. L., Li, H. B., Tang, Q. X., Tong, Y. H. & Liu, Y. C. A facile post-peeling modification approach of elastic dielectrics for high-performance conformal organic thin-film transistors. *J. Mater. Chem. C.* **7**, 3199–3205 (2019).
221. Ding, Z. Q. et al. Effect of oxygen, moisture and illumination on the stability and reliability of dinaphtho[2,3-b:2′,3′-f]thieno[3,2-b]thiophene (DNTT) OTFTs during operation and storage. *ACS Appl. Mater. Interfaces.* **6**, 15224–15231 (2014).
222. Hosono, H., Kikuchi, N., Ueda, N. & Kawazoe, H. Working hypothesis to explore novel wide band gap electrically conducting amorphous oxides and examples. *J. Non-Cryst. Solids* **200**, 165–169 (1996).
223. Zulqarnain, M. et al. Design trade-offs in amorphous indium gallium zinc oxide thin film transistor based bio-signal sensing front-ends. *Flex. Print. Electron.* **4**, 014001 (2019).
224. Petti, L. et al. Gain-tunable complementary common-source amplifier based on a flexible hybrid thin-film transistor technology. *IEEE Electron Device Lett.* **38**, 1536–1539 (2017).
225. Zulqarnain, M. et al. A flexible ECG patch compatible with NFC RF communication. *NPJ Flex. Electron.* **4**, 13 (2020).
226. Mao, S. S., Li, J., Guo, A. Y., Zhao, T. T. & Zhang, J. H. An active multielectrode array for collecting surface electromyogram signals using a-IGZO TFT technology on polyimide substrate. *IEEE Trans. Electron Devices* **67**, 1613–1618 (2020).
227. Wang, B. et al. Flexible and stretchable metal oxide nanofiber networks for multimodal and monolithically integrated wearable electronics. *Nat. Commun.* **11**, 2405–2416 (2020).
228. Luo, Z. et al. Sub-thermionic, ultra-high-gain organic transistors and circuits. *Nat. Commun.* **12**, 1928–1937 (2021).
229. Huang, T. C. et al. Pseudo-CMOS: a design style for low-cost and robust flexible electronics. *IEEE Trans. Electron Devices* **58**, 141–150 (2011).
230. Jeong, D. Y., Chang, Y., Yoon, W. G., Do, Y. & Jang, J. Low-temperature polysilicon oxide thin-film transistors with coplanar structure using six photomask steps demonstrating high inverter gain of 264 V/V. *Adv. Eng. Mater.* **22**, 1901497 (2020).
231. Kim, H., Jeong, D. Y., Lee, S. & Jang, J. A high-gain inverter with low-temperature poly-si oxide thin-film transistors. *IEEE Electron Device Lett.* **40**, 411–414 (2019).
232. Yang, C. Y. et al. Low-power/high-gain flexible complementary circuits based on printed organic electrochemical transistors. *Adv. Electron. Mater.* **8**, 2100907 (2021).
233. Jeon, D. H., Jeong, W. B., Park, J. S., Chung, H. J. & Lee, S. W. A high-gain two-stage amplifier using low-temperature poly-si oxide thin-film transistors with a Corbino structure. *J. Inf. Disp.* **23**, 281–286 (2022).
234. Rahaman, A., Jeong, H. & Jang, J. A high-gain CMOS operational amplifier using low-temperature poly-si oxide TFTs. *IEEE Trans. Electron Devices* **67**, 524–528 (2020).
235. Kim, M. K. et al. Flexible submental sensor patch with remote monitoring controls for management of oropharyngeal swallowing disorders. *Sci. Adv.* **5**, eaay3210 (2019).
236. Farina, D. et al. Man/machine interface based on the discharge timings of spinal motor neurons after targeted muscle reinnervation. *Nat. Biomed. Eng.* **1**, 0025 (2017).
237. Inzelberg, L., Rand, D., Steinberg, S., David-Pur, M. & Hanein, Y. A wearable high-resolution facial electromyography for long term recordings in freely behaving humans. *Sci. Rep.* **8**, 2058 (2018).
238. Lee, H. et al. Stretchable array electromyography sensor with graph neural network for static and dynamic gestures recognition system. *NPJ Flex. Electron.* **7**, 20 (2023).

ACKNOWLEDGEMENTS

The authors would like to acknowledge the financial support given by the National Natural Science Foundation of China (52227808), the National Science Foundation for Distinguished Young Scholars of China (51725505), Shanghai Science and Technology Commission (19JC1412400), and the Development Fund for Shanghai Talents (2021003).

AUTHOR CONTRIBUTIONS

J.L. and A.Y.G. conceptualized the work; L.C. and J.L. collected the data and contributed to the scientific discussions; L.C. wrote the first draft of the manuscript; editing and revision were carried out by J.L. and J.H.Z.

COMPETING INTERESTS

The authors declare no competing interests.

ADDITIONAL INFORMATION

Correspondence and requests for materials should be addressed to Jun Li or Jianhua Zhang.